HAL
open science

A bending-gradient model for thick plates, I : theory

Arthur Lebée, Karam Sab

To cite this version:

Arthur Lebée, Karam Sab. A bending-gradient model for thick plates, I : theory. International Journal of Solids and Structures, 2011, 48, pp.2878-2888. 10.1016/j.ijsolstr.2011.06.006 . hal-00661326

HAL Id: hal-00661326

https://enpc.hal.science/hal-00661326v1

Submitted on 18 Apr 2012

HAL is a multi-disciplinary open access archive for the deposit and dissemination of scientific research documents, whether they are published or not. The documents may come from teaching and research institutions in France or abroad, or from public or private research centers.

L'archive ouverte pluridisciplinaire **HAL**, est destinée au dépôt et à la diffusion de documents scientifiques de niveau recherche, publiés ou non, émanant des établissements d'enseignement et de recherche français ou étrangers, des laboratoires publics ou privés.

A Bending-Gradient model for thick plates, Part I: Theory

A. Lebée, K. Sab*

Université Paris-Est, Laboratoire Navier (ENPC/IFSTTAR/CNRS).
École des Ponts ParisTech, 6 et 8 avenue Blaise Pascal.
77455 Marne-la-Vallée, France
tel.+33-1-64153749, fax.+33-1-64153741,
e-mail: arthur.lebee@lami.enpc.fr, sab@enpc.fr

Abstract

This is the first part of a two-part paper dedicated to a new plate theory for out-of-plane loaded thick plates where the static unknowns are those of the Kirchhoff-Love theory (3 in-plane stresses and 3 bending moments), to which six components are added representing the gradient of the bending moment. The new theory, called the Bending-Gradient plate theory is described in the present paper. It is an extension to arbitrarily layered plates of the Reissner-Mindlin plate theory which appears as a special case of the Bending-Gradient plate theory when the plate is homogeneous. However, we demonstrate also that, in the general case, the Bending-Gradient model cannot be reduced to a Reissner-Mindlin model. In part two (Lebée and Sab, 2010a), the Bending-Gradient theory is applied to multilayered plates and its predictions are compared to those of the Reissner-Mindlin theory and to full 3D Pagano's exact solutions. The main conclusion of the second part is that the Bending-Gradient gives good predictions of both deflection and shear stress distributions in any material configuration. Moreover, under some symmetry conditions, the Bending-Gradient model coincides with the second-order approximation of the exact solution as the slenderness ratio L/h goes to infinity.

Key words: Plate Theory, Higher-order Models, Laminated Plates, Composite Plates

1. Introduction

Laminated composite plates are widely used in engineering applications, especially in aeronautics. They offer excellent stiffness and strength performance for a low density. However, as fiber reinforced composites are very anisotropic materials, the overall plate properties of these laminates has been really difficult to capture. Because of a strong demand from industry for reliable models, many suggestions have been made.

Let us recall some essential requirements for such a model. The main goal is to simplify a computationally heavy 3D model into a 2D plate model without losing local 3D fields' accuracy. One would expect:

1. Good estimation of macroscopic deflection,
2. No limitation on local material symmetries,
3. A plate theory which is easy to implement with standard finite element tools,
4. Good relocalization of 3D fields in order to estimate local stresses.

The simplest and most widely-used theory is the Kirchhoff-Love plate model. This model is easy to implement and gives good estimates for in-plane stress components (far from the edges of the plate) and neglects the contribution of out-of-plane stress components to the stress energy. However, when the plate slenderness ratio L/h (h is the plate thickness and L the span) is not large enough, out-of-plane stresses have an increasing influence on the plate deflection. This phenomenon becomes sensitive when $L/h < 10$ for an isotropic plate and $L/h < 40$ for classical carbon fiber reinforced laminated plates and cannot be neglected for conventional use of composite laminates.

In recent decades many suggestions have been made to improve both deflection estimation and field localization for highly heterogeneous laminates. Reddy (1989), Noor and Malik (2000) and Carrera (2002) provided detailed reviews for these models. Two main approaches can be found: asymptotic approaches and axiomatic approaches. The first one is mainly based on the fact that h/L is a small parameter. Using asymptotic expansions in the small parameter h/L (Caillerie, 1984; Lewinski, 1991c,b,a), it is found that the Kirchhoff-Love kinematic is actually the first order of the expansion. However, higher-order terms yield only intricated "Kirchhoff-Love" plate equations and no simple model to implement. This difficulty is illustrated in (Boutin, 1996) for 3D periodic composites and in Buannic and Cartraud (2001a,b) for periodic beams. Another asymptotic method is based on the so-called Variational Asymptotic Method (VAM) applied to plates by Yu et al. (2002b,a). The strength of this approach is that it does not make more assumption than having h/L small and, according to its authors, it could be applied also to any non-linearities. However, this method does not seem simple to implement in conventional finite element code.

The second main approach is based on assuming *ad hoc* displacement or stress 3D fields and often referred to as axiomatic approach. One of the assets of these approaches is that they seem easier to implement in finite element codes. These models can be "Equivalent Single Layer" or "Layerwise".

Equivalent Single Layer models treat the whole laminate as an equivalent homogeneous plate. Stress or displacement approaches have been suggested. Reissner (1945) was the first one who suggested a stress approach for homogeneous and isotropic plates. His approach will be detailled further in the present work. Reissner's transverse shear stress field is a parabolic distribution through the thickness. However, experiments and some exact solutions (Pagano, 1969, 1970a,b) when considering composite laminates, revealed that shear stress distributions are much more distorted than that. At the same time, numerous displacement approaches were suggested. The roughest suggestion for taking into account transverse shear strains, $\varepsilon_{\alpha 3}$, is assuming that $\varepsilon_{\alpha 3}$ is uniform through the thickness (First Order Shear Deformation Theory). Yet, it leads to too stiff shear behavior and necessitates the introduction of shear correction factors (Mindlin (1951) and Whitney (1972)). Above all, this assumption enforces a discontinuous shear stress $\sigma_{\alpha 3}$ through the thickness. Other models have been designed (Reddy, 1984; Touratier, 1991; Vidal and Polit, 2008) to remove the use of shear correction factors, but most of them did not lead to continuous $\sigma_{\alpha 3}$, as indicated by Reddy (1989). The most refined Equivalent Single Layers models, which finally led to continuous shear stress are zigzag models (Ambartsumian, 1969; Whitney, 1969; Carrera, 2003). However, these models are restricted to some specific configurations (symmetry of the plate and material constitutive equation) and involve higher-order partial derivative equations than the simple Reissner-Mindlin plate model.

The difficulties encountered with transverse stress fields instigated the consideration of enriched models: Layerwise models. In these models, all plate degrees of freedom are introduced in each layer of the laminate. Continuity conditions are enforced between layers. In this area, most of the improvements have been focused on refining the local displacement field. The reader can refer to Reddy (1989) and Carrera (2002) for detailed reviews. It should be noted that a static approach has also been considered for layerwise models. Based on the variational formulation from Pagano (1978), it treats each layer as a Reissner-Mindlin plate and enforces stress continuity conditions (Naciri et al., 1998; Diaz Diaz et al., 2001; Hadj-Ahmed et al., 2001; Caron et al., 2006; Diaz Diaz et al., 2007; Dallot and Sab, 2008). Both stress and displacement approaches for Layerwise models lead to correct estimates of local 3D fields. However their main drawback is that they involve many more degrees of freedom (proportional to the number of layers) than Equivalent Single Layer models.

Based on Reissner (1945) paper, the purpose of this work is to suggest an Equivalent Single Layer higher-order plate theory which gives an accurate enough estimate of transverse shear stresses in the linear elasticity framework. For this, we are motivated by two observations. The first one is that Kirchhoff-Love strain fields have clearly been identified as good first-order approximation for slender plates thanks to asymptotic expansion approaches. Thus, it would be inconsistent to refine in-plane fields further without introducing correct estimation of transverse fields. The second one is that the 3D equilibrium plays a critical role in the estimation of transverse shear stress in all the existing approaches. For instance, Whitney (1972) introduced 3D equilibrium in order to compute shear correction factors and more recently, when benchmarking several plate models, Noor and Malik (2000) used the 3D equilibrium to estimate shear stresses. We show in this paper that revisiting the use of 3D equilibrium in order to derive transverse shear stress as Reissner (1945) did for homogeneous plates leads to a full bending gradient plate theory. The Reissner-Mindlin theory will

appear as a special case of the new Bending-Gradient theory when the plate is homogeneous.

The paper is organized as follows. In Section 2 notations are introduced. In Section 3 we recall briefly the full 3D elastic problem for a clamped plate and, in Section 4, how it is possible to derive plate equilibrium equations without any assumption on microscopic fields and how Reissner derived his shear stress distribution. Then we demonstrate in Section 5.1.1 that applying Reissner's approach for deriving transverse shear stress to a composite laminate involves more static shear degrees of freedom (DOF) than the usual shear forces $\boldsymbol{Q}$. The mechanical meaning of these new DOF is presented and compatible fields are identified in Section 5.2. The constitutive equation for the bending gradient is derived in Section 5.3 which leads to the formulation of a complete plate theory. Finally, in Section 6, it is demonstrated that for the special case of homogeneous plates, the Reissner-Mindlin and the Bending-Gradient plate theory are identical. Thus a means to quantitatively compare both theories is provided and applied to conventional laminates.

2. Notations

Vectors and higher-order tensors are boldfaced and different typefaces are used for each order: vectors are slanted: $\boldsymbol{T}$, $\boldsymbol{u}$. Second order tensors are sans serif: M, e. Third order tensors are in typewriter style: $\mathtt{\Phi}$, $\mathtt{\Gamma}$. Fourth order tensors are in calligraphic style $\boldsymbol{\mathcal{D}}$, $\boldsymbol{\mathcal{c}}$. Sixth order tensors are double stroked $\mathbb{F}$, $\mathbb{W}$.

When dealing with plates, both 2-dimensional (2D) and 3D tensors are used. Thus, $\tilde{\boldsymbol{T}}$ denotes a 3D vector and $\boldsymbol{T}$ denotes a 2D vector or the in-plane part of $\tilde{\boldsymbol{T}}$. The same notation is used for higher-order tensors: $\tilde{\boldsymbol{\sigma}}$ is the 3D second-order stress tensor while $\boldsymbol{\sigma}$ is its in-plane part. When dealing with tensor components, the indexes specify the dimension: a_{ij} denotes the 3D tensor $\tilde{\mathsf{a}}$ with Latin index $i, j, k.. = 1, 2, 3$ and $\mathsf{a}_{\alpha\beta}$ denotes the 2D tensor a with Greek indexes $\alpha, \beta, \gamma.. = 1, 2$. $\tilde{\boldsymbol{\mathcal{C}}} = \mathcal{C}_{ijkl}$ is the fourth-order 3D elasticity stiffness tensor. $\tilde{\boldsymbol{\mathcal{S}}} = \mathcal{S}_{ijkl} = \tilde{\boldsymbol{\mathcal{C}}}^{-1}$ is the fourth-order 3D elasticity compliance tensor while $\boldsymbol{\mathcal{c}} = \mathcal{c}_{\alpha\beta\gamma\delta}$ denotes the plane-stress elasticity tensor. $\boldsymbol{\mathcal{c}}$ is not the in-plane part of $\tilde{\boldsymbol{\mathcal{C}}}$ but it is the inverse of the in-plane part of $\tilde{\boldsymbol{\mathcal{S}}}$: $\boldsymbol{\mathcal{c}} = \boldsymbol{\mathcal{S}}^{-1}$. The identity for in-plane elasticity is $\mathcal{i}_{\alpha\beta\gamma\delta} = \frac{1}{2}\left(\delta_{\alpha\gamma}\delta_{\beta\delta} + \delta_{\alpha\delta}\delta_{\beta\gamma}\right)$, where $\delta_{\alpha\beta}$ is Kronecker symbol ($\delta_{\alpha\beta} = 1$ if $\alpha = \beta$, $\delta_{\alpha\beta} = 0$ otherwise).

The transpose operation ${}^t\bullet$ is applied to any order tensors as follows: $\left({}^tA\right)_{\alpha\beta\ldots\psi\omega} = A_{\omega\psi\ldots\beta\alpha}$.

Three contraction products are defined, the usual dot product ($\tilde{\boldsymbol{a}} \cdot \tilde{\boldsymbol{b}} = a_i b_i$), the double contraction product ($\tilde{\boldsymbol{a}} : \tilde{\boldsymbol{b}} = a_{ij} b_{ji}$) and a triple contraction product ($\mathtt{A} \therefore \mathtt{B} = \mathtt{A}_{\alpha\beta\gamma}\mathtt{B}_{\gamma\beta\alpha}$). Einstein's notation on repeated indexes is used in these definitions. It should be noticed that closest indexes are summed together in contraction products. Thus, $\mathtt{\Phi} \cdot \boldsymbol{n} = \mathtt{\Phi}_{\alpha\beta\gamma} n_\gamma$ is different from $\boldsymbol{n} \cdot \mathtt{\Phi} = n_\alpha \mathtt{\Phi}_{\alpha\beta\gamma}$. The reader might easily check that $\boldsymbol{i} : \boldsymbol{i} = \boldsymbol{i}$, $\boldsymbol{i} \therefore \boldsymbol{i} = 3/2\,\boldsymbol{\delta}$ and that $\boldsymbol{i} \cdot \boldsymbol{i} = \mathcal{i}_{\alpha\beta\gamma\delta}\mathcal{i}_{\delta\epsilon\zeta\eta}$ is a sixth-order tensor. We recall also that resp. $\boldsymbol{a} \cdot \boldsymbol{b}$, ${}^t\boldsymbol{a} : \boldsymbol{b}$ and ${}^t\mathtt{a} \therefore \mathtt{b}$ define inner products and associated norms on $\mathbb{R}^2$, $\left(\mathbb{R}^2\right)^2$ and $\left(\mathbb{R}^2\right)^3$, respectively.

The derivation operator $\tilde{\boldsymbol{\nabla}}$ is also formally represented as a vector: $\tilde{\boldsymbol{a}} \cdot \tilde{\boldsymbol{\nabla}} = \mathsf{a}_{ij}\nabla_j = \mathsf{a}_{ij,j}$ is the divergence and $\boldsymbol{a} \otimes \boldsymbol{\nabla} = \mathsf{a}_{\alpha\beta}\nabla_\gamma = \mathsf{a}_{\alpha\beta,\gamma}$ is the gradient. Here $\otimes$ is the dyadic product.

Finally, the integration through the thickness is noted $\langle\bullet\rangle$: $\int_{-\frac{h}{2}}^{\frac{h}{2}} f(x_3)dx_3 = \langle f \rangle$.

3. The 3D model

We consider a linear elastic plate of thickness h occupying the 3D domain $\Omega = \omega \times]-h/2, h/2[$, where $\omega \subset \mathbb{R}^2$ is the mid-plane of the plate (Figure 1). Cartesian coordinates (x_1, x_2, x_3) in the reference frame $(\tilde{\boldsymbol{e}}_1, \tilde{\boldsymbol{e}}_2, \tilde{\boldsymbol{e}}_3)$ are used. The constitutive material is assumed to be invariant with respect to translations in the (x_1, x_2) plane. Hence, the stiffness tensor $\tilde{\boldsymbol{\mathcal{C}}}$ is a function of x_3 only. The plate is loaded on its upper and lower faces $\omega^\pm = \omega \times \{\pm h/2\}$ with the distributed force $\tilde{\boldsymbol{T}}^\pm$. There are no body forces and the plate is clamped on its lateral edge, $\partial\omega \times]-h/2, h/2[$ where $\partial\omega$ is the edge of ω.

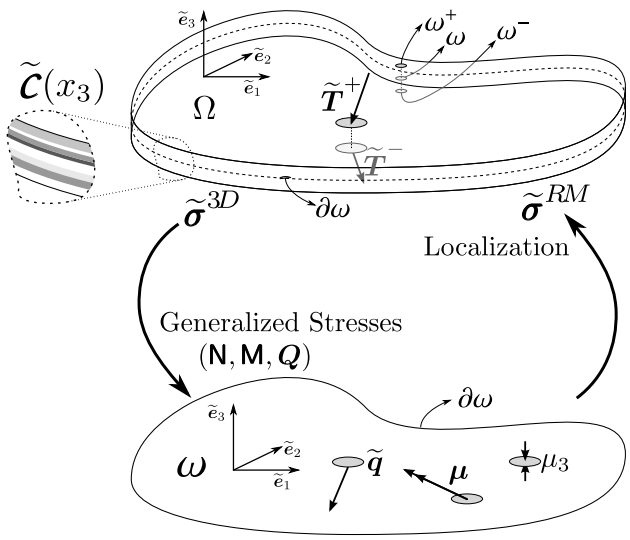

Figure 1: The Plate Configuration

The 3D problem $\mathcal{P}^{3D}$ is summarized as follows:

$$\mathcal{P}^{3D}\begin{cases} \tilde{\boldsymbol{\sigma}} \cdot \tilde{\boldsymbol{\nabla}} = 0 \quad \text{on } \Omega. & \text{(1a)} \\ \tilde{\boldsymbol{\sigma}} = \tilde{\boldsymbol{\mathcal{C}}}(x_3) : \tilde{\boldsymbol{\varepsilon}} \quad \text{on } \Omega. & \text{(1b)} \\ \tilde{\boldsymbol{\sigma}} \cdot \tilde{\boldsymbol{e}}_3 = \tilde{\boldsymbol{T}}^{\pm} \quad \text{on } \omega^{\pm}. & \text{(1c)} \\ \tilde{\boldsymbol{\varepsilon}} = \dfrac{1}{2}\left(\tilde{\boldsymbol{\nabla}} \otimes \tilde{\boldsymbol{u}} + \tilde{\boldsymbol{u}} \otimes \tilde{\boldsymbol{\nabla}}\right) \quad \text{on } \Omega. & \text{(1d)} \\ \tilde{\boldsymbol{u}} = 0 \quad \text{on } \partial\omega \times]-h/2, h/2[. & \text{(1e)} \end{cases}$$

where $\tilde{\boldsymbol{u}}$ is the 3D displacement vector field, $\tilde{\boldsymbol{\varepsilon}}$ is the strain tensor field and $\tilde{\boldsymbol{\sigma}}$ is the stress tensor field. It is useful to recall the variational approach for the problem $\mathcal{P}^{3D}$. The sets of statically compatible stress fields SC^{3D} and kinematically compatible strain fields KC^{3D} are introduced. SC^{3D} is the set of stress fields $\tilde{\boldsymbol{\sigma}}$ which comply with equilibrium equation (1a) and boundary condition on the upper and lower faces of the plate (1c). KC^{3D} is the set of strain fields $\tilde{\boldsymbol{\varepsilon}}$ which derive from a continuous displacement field $\tilde{\boldsymbol{u}}$ (Equation 1d) and comply with boundary condition on the edge of the plate (1e).

The strain and stress energy density w^{3D} and w^{*3D} are respectively given by:

$$w^{3D}\left(\tilde{\boldsymbol{\varepsilon}}\right) = \frac{1}{2}\,\tilde{\boldsymbol{\varepsilon}} : \tilde{\boldsymbol{\mathcal{C}}} : \tilde{\boldsymbol{\varepsilon}}, \qquad w^{*3D}\left(\tilde{\boldsymbol{\sigma}}\right) = \frac{1}{2}\,\tilde{\boldsymbol{\sigma}} : \tilde{\boldsymbol{\mathcal{S}}} : \tilde{\boldsymbol{\sigma}} \tag{2}$$

They are related by the following Legendre-Fenchel transform:

$$w^{*3D}\left(\tilde{\boldsymbol{\sigma}}\right) = \sup_{\tilde{\boldsymbol{\varepsilon}}} \left\{\tilde{\boldsymbol{\sigma}} : \tilde{\boldsymbol{\varepsilon}} - w^{3D}\left(\tilde{\boldsymbol{\varepsilon}}\right)\right\} \tag{3}$$

The kinematic variational approach states that the strain solution $\tilde{\boldsymbol{\varepsilon}}^{3D}$ of $\mathcal{P}^{3D}$ is the one that minimizes P^{3D} among all kinematically compatible strain fields:

$$P^{3D}\left(\tilde{\boldsymbol{\varepsilon}}^{3D}\right) = \min_{\tilde{\boldsymbol{\varepsilon}} \in KC^{3D}} \left\{P^{3D}\left(\tilde{\boldsymbol{\varepsilon}}\right)\right\} \tag{4}$$

where P^{3D} is the potential energy given by:

$$P^{3D}\left(\tilde{\boldsymbol{\varepsilon}}\right) = \int_{\Omega} w^{3D}\left(\tilde{\boldsymbol{\varepsilon}}\right) d\Omega - \int_{\omega} \tilde{\boldsymbol{T}}^{+} \cdot \tilde{\boldsymbol{u}}^{+} + \tilde{\boldsymbol{T}}^{-} \cdot \tilde{\boldsymbol{u}}^{-} d\omega \tag{5}$$

and $\tilde{\boldsymbol{u}}^{\pm} = \tilde{\boldsymbol{u}}(x_1, x_2, \pm h/2)$ are the 3D displacement fields on the upper and lower faces of the plate.

The static variational approach states that the stress solution $\tilde{\boldsymbol{\sigma}}^{3D}$ of $\mathcal{P}^{3D}$ is the one that minimizes P^{*3D} among all statically compatible stress fields:

$$P^{*3D}\left(\tilde{\boldsymbol{\sigma}}^{3D}\right) = \min_{\tilde{\boldsymbol{\sigma}} \in \mathcal{SC}^{3D}} \left\{P^{*3D}\left(\tilde{\boldsymbol{\sigma}}\right)\right\} \tag{6}$$

where P^{*3D} is the complementary potential energy given by:

$$P^{*3D}\left(\tilde{\boldsymbol{\sigma}}\right) = \int_{\Omega} w^{*3D}\left(\tilde{\boldsymbol{\sigma}}\right) d\Omega \tag{7}$$

Moreover, the following relation holds for the solution:

$$P^{3D}\left(\tilde{\boldsymbol{\varepsilon}}^{3D}\right) = -P^{*3D}\left(\tilde{\boldsymbol{\sigma}}^{3D}\right) \Leftrightarrow V_{ext}^{3D} = V_{int}^{3D} \tag{8}$$

where the external work is:

$$V_{ext}^{3D} = \int_{\omega} \tilde{\boldsymbol{T}}^{+} \cdot \tilde{\boldsymbol{u}}^{3D+} + \tilde{\boldsymbol{T}}^{-} \cdot \tilde{\boldsymbol{u}}^{3D-} d\omega, \tag{9}$$

and the internal work is:

$$V_{int}^{3D} = \int_{\Omega} \tilde{\boldsymbol{\sigma}}^{3D} : \tilde{\boldsymbol{\varepsilon}}^{3D} d\Omega. \tag{10}$$

4. Revisiting the Reissner-Mindlin plate theory

4.1. Reissner-Mindlin statically compatible fields

This section recalls shortly the procedure for the derivation of Reissner-Mindlin equilibrium equations (Reissner, 1945; Mindlin, 1951; Caron and Sab, 2001; Nguyen et al., 2005).

The generalized Reissner-Mindlin stresses associated to the 3D stress field $\tilde{\boldsymbol{\sigma}}$ are:

$$\begin{cases} N_{\alpha\beta}\left(x_1, x_2\right) = \langle \sigma_{\alpha\beta} \rangle & \text{(11a)} \\ M_{\alpha\beta}\left(x_1, x_2\right) = \langle x_3 \sigma_{\alpha\beta} \rangle & \text{(11b)} \\ Q_{\alpha}\left(x_1, x_2\right) = \langle \sigma_{\alpha 3} \rangle & \text{(11c)} \end{cases}$$

where $\boldsymbol{N}$ is the membrane stress, $\boldsymbol{M}$ the bending moment, and $\boldsymbol{Q}$ the shear forces.

Reissner-Mindlin equilibrium equations are obtained by integrating equations (1a) and $x_3 \times$(1a) with respect to x_3 leading to:

$$\begin{cases} \langle \sigma_{\alpha\beta,\beta} \rangle + \left[\sigma_{\alpha 3}\right]_{-h/2}^{h/2} = 0 \\ \langle \sigma_{\alpha 3,\alpha} \rangle + \left[\sigma_{33}\right]_{-h/2}^{h/2} = 0 \\ \langle x_3 \sigma_{\alpha\beta,\beta} \rangle - \langle \sigma_{\alpha 3} \rangle + \left[x_3 \sigma_{\alpha 3}\right]_{-h/2}^{h/2} = 0 \end{cases}$$

Using boundary conditions (1c) yields:

$$\begin{cases} N_{\alpha\beta,\beta} + p_{\alpha} = 0 & \text{(12a)} \\ Q_{\alpha,\alpha} + p_3 = 0 & \text{(12b)} \\ M_{\alpha\beta,\beta} - Q_{\alpha} + \mu_{\alpha} = 0 & \text{(12c)} \end{cases}$$

where $p_i = T_i^{+} + T_i^{-}$ are symmetric loadings per unit surface and $\mu_i = \frac{h}{2}(T_i^{+} - T_i^{-})$ are skew-symmetric loadings per unit surface. More precisely, $\boldsymbol{p} = (p_{\alpha})$ are membrane loadings per unit surface, p_3 is the out-of-plane loading per unit surface, $\boldsymbol{\mu} = (\mu_{\alpha})$ are couples per unit surface and μ_3 is the transverse bulk loading.

Since in-plane loadings ($\boldsymbol{p}$, $\boldsymbol{\mu}$) and out-of-plane loadings (p_3, μ_3) are not of the same order in the asymptotic analysis of the plate as h/L goes to 0 (see Lewinski (1991c)), and for the sake of simplicity, we focus only on the out-of-plane loading p_3 ($p_\alpha = \mu_i = 0$).

Finally, for clamped plates, SC^{RM} is the set of statically compatible $(\boldsymbol{N}, \boldsymbol{M}, \boldsymbol{Q})$ fields defined by:

$$(\boldsymbol{N}, \boldsymbol{M}, \boldsymbol{Q}) \in SC^{RM} \Leftrightarrow \begin{cases} \boldsymbol{N} \cdot \boldsymbol{\nabla} = \mathbf{o} \text{ on } \omega & \text{(13a)} \\ \boldsymbol{M} \cdot \boldsymbol{\nabla} - \boldsymbol{Q} = \mathbf{o} \text{ on } \omega & \text{(13b)} \\ \boldsymbol{Q} \cdot \boldsymbol{\nabla} + q_3 = 0 \text{ on } \omega & \text{(13c)} \end{cases}$$

4.2. Localization

The second step of the static approach consists in deriving the Reissner-Mindlin stress energy per unit surface $w^{*RM}(\boldsymbol{N}, \boldsymbol{M}, \boldsymbol{Q})$ from the 3D model. Then, the solution for the Reissner-Mindlin model is obtained by minimizing the complementary potential energy $P^{*RM} = \int_\omega w^{*RM} d\omega$ over all $(\boldsymbol{N}, \boldsymbol{M}, \boldsymbol{Q})$ in SC^{RM}.

As in many homogenization procedures, the derivation of w^{*RM} is based on an approximation scheme for the real 3D stress fields in terms of Reissner-Mindlin stress fields:

$$\tilde{\boldsymbol{\sigma}}^{RM}(x_1, x_2, x_3) = \tilde{\boldsymbol{\sigma}}^{(N)}(x_1, x_2, x_3) + \tilde{\boldsymbol{\sigma}}^{(M)}(x_1, x_2, x_3) + \tilde{\boldsymbol{\sigma}}^{(Q)}(x_1, x_2, x_3)$$

where $\tilde{\boldsymbol{\sigma}}^{(N)}$, $\tilde{\boldsymbol{\sigma}}^{(M)}$, and $\tilde{\boldsymbol{\sigma}}^{(Q)}$ are 3D stress fields generated by $\boldsymbol{N}$, $\boldsymbol{M}$ and $\boldsymbol{Q}$ as follows:

$$\begin{cases} \sigma_{ij}^{(N)} = s_{ij\alpha\beta}^{(N)}(x_3) N_{\alpha\beta}(x_1, x_2) & \text{(14a)} \\ \sigma_{ij}^{(M)} = s_{ij\alpha\beta}^{(M)}(x_3) M_{\alpha\beta}(x_1, x_2) & \text{(14b)} \\ \sigma_{ij}^{(Q)} = s_{ij\alpha}^{(Q)}(x_3) Q_\alpha(x_1, x_2) & \text{(14c)} \end{cases}$$

where $s_{ij\alpha\beta}^{(N)}(x_3)$, $s_{ij\alpha\beta}^{(M)}(x_3)$ and $s_{ij\alpha}^{(Q)}(x_3)$ are localization tensors depending only on the x_3 coordinate. This can be rewritten using contraction products as:

$$\tilde{\boldsymbol{\sigma}}^{RM} = \tilde{\boldsymbol{s}}^{(N)} : \boldsymbol{N} + \tilde{\boldsymbol{s}}^{(M)} : \boldsymbol{M} + \tilde{\boldsymbol{s}}^{(Q)} \cdot \boldsymbol{Q}$$

Once this approximation of stress fields is set, the stress potential energy density $w^{*RM}(\boldsymbol{N}, \boldsymbol{M}, \boldsymbol{Q})$ is defined simply as the quadratic form:

$$w^{*RM}(\boldsymbol{N}(x_1, x_2), \boldsymbol{M}(x_1, x_2), \boldsymbol{Q}(x_1, x_2)) = \frac{1}{2} \left\langle \tilde{\boldsymbol{\sigma}}^{RM}(x_1, x_2, x_3) : \tilde{\boldsymbol{\mathcal{S}}}(x_3) : \tilde{\boldsymbol{\sigma}}^{RM}(x_1, x_2, x_3) \right\rangle \tag{15}$$

Hence, a consistent choice for $\tilde{\boldsymbol{s}}^{(N)}$, $\tilde{\boldsymbol{s}}^{(M)}$ and $\tilde{\boldsymbol{s}}^{(Q)}$ is critical.

4.2.1. Kirchhoff-Love fields

The derivation of $\tilde{\boldsymbol{s}}^{(N)}$ and $\tilde{\boldsymbol{s}}^{(M)}$ is based on the Kirchhoff-Love plate theory. This theory is the first order of asymptotic expansion in the small parameter h/L (Ciarlet and Destuynder, 1979; Caillerie, 1984). According to this theory, plane-stress is assumed and the in-plane part of the displacement is linear in x_3:

$$u_\alpha^{KL} = U_\alpha - x_3 U_{3,\alpha} \tag{16}$$

where U_α is the average in-plane displacement and U_3 the average out-of-plane displacement (the deflection). From this, the in-plane strains are derived as:

$$\boldsymbol{\varepsilon}^{KL} = \frac{1}{2}\left(U_{\alpha,\beta} + U_{\beta,\alpha}\right) - x_3 U_{3,\alpha\beta} = \boldsymbol{e} + x_3 \boldsymbol{\kappa} \tag{17}$$

where $\boldsymbol{e}$ is the membrane strain and $\boldsymbol{\kappa}$ the curvature at first order. We draw the reader's attention to the fact that strain components ε_{i3} are not null in the general case.

Membrane stress $\boldsymbol{N}$ and bending moments $\boldsymbol{M}$ are linearly dependent on $\boldsymbol{e}$ and $\boldsymbol{\kappa}$:

$$\begin{cases} \boldsymbol{N} = \boldsymbol{\mathcal{A}} : \boldsymbol{e} + \boldsymbol{\mathcal{B}} : \boldsymbol{\kappa} & \text{(18a)} \\ \boldsymbol{M} = {}^t\boldsymbol{\mathcal{B}} : \boldsymbol{e} + \boldsymbol{\mathcal{D}} : \boldsymbol{\kappa} & \text{(18b)} \end{cases}$$

with:

$$(\boldsymbol{\mathcal{A}}, \boldsymbol{\mathcal{B}}, \boldsymbol{\mathcal{D}}) = \left\langle \left(1, x_3, x_3^2\right) \boldsymbol{c}(x_3) \right\rangle \tag{19}$$

Using 3D constitutive equation under plane-stress assumption, Kirchhoff-Love constitutive equation (18) and in-plane strains definition (17), it is possible to express Kirchhoff-Love stress fields as functions of $\boldsymbol{N}$ and $\boldsymbol{M}$:

$$\begin{cases} \boldsymbol{\sigma}^{(N)}(x_1, x_2, x_3) = \boldsymbol{c}(x_3) : \left(\boldsymbol{a} + x_3\, {}^t\boldsymbol{b}\right) : \boldsymbol{N}(x_1, x_2) \quad \text{and } \sigma_{i3}^{(N)} = 0 & \text{(20a)} \\ \boldsymbol{\sigma}^{(M)}(x_1, x_2, x_3) = \boldsymbol{c}(x_3) : (\boldsymbol{b} + x_3\, \boldsymbol{d}) : \boldsymbol{M}(x_1, x_2) \quad \text{and } \sigma_{i3}^{(M)} = 0 & \text{(20b)} \end{cases}$$

where $\boldsymbol{a}$, $\boldsymbol{b}$ and $\boldsymbol{d}$ are the reciprocal compliance tensors of the constitutive equation (18):

$$\begin{cases} \boldsymbol{e} = \boldsymbol{a} : \boldsymbol{N} + \boldsymbol{b} : \boldsymbol{M} & \text{(21a)} \\ \boldsymbol{\kappa} = {}^t\boldsymbol{b} : \boldsymbol{N} + \boldsymbol{d} : \boldsymbol{M} & \text{(21b)} \end{cases}$$

Hence, for a homogeneous plate, Kirchhoff-Love stress fields are given by:

$$\begin{cases} \boldsymbol{\sigma}^{(N)}(x_1, x_2, x_3) = \dfrac{1}{h}\boldsymbol{N}(x_1, x_2) \quad \text{and } \sigma_{i3}^{(N)} = 0 & \text{(22a)} \\ \boldsymbol{\sigma}^{(M)}(x_1, x_2, x_3) = \dfrac{12x_3}{h^3}\boldsymbol{M}(x_1, x_2) \quad \text{and } \sigma_{i3}^{(M)} = 0 & \text{(22b)} \end{cases}$$

4.2.2. Shear fields for a homogeneous plate

Let us recall the approach from Reissner (1945) for deriving $\tilde{\boldsymbol{\sigma}}^{(Q)}$ in the case of a homogeneous monoclinic[1] plate.

The main idea of the method is to recall that the shear forces are related to the bending moment through the plate equilibrium (13b). In the previous section, 3D fields generated by a (x_1, x_2)-invariant bending moment have been derived (Equation 22). If $\boldsymbol{M}$ is invariant, we have $\tilde{\boldsymbol{\sigma}}^{(M)} \cdot \tilde{\boldsymbol{\nabla}} = \tilde{\mathbf{o}}$. However, if $\boldsymbol{M}$ is function of x_1 and x_2, $\tilde{\boldsymbol{\sigma}}^{(M)}$ field is no more equilibrated and it comes directly: $\boldsymbol{\sigma}^{(M)} \cdot \boldsymbol{\nabla} = \frac{12x_3}{h^3}\left(\boldsymbol{M} \cdot \boldsymbol{\nabla}\right) = \frac{12x_3}{h^3}\boldsymbol{Q}$. $\boldsymbol{f}^{(Q)} = \frac{12x_3}{h^3}\boldsymbol{Q}$ appears as the body force generated by the bending moment variations and is directly proportional to shear forces. Then $\tilde{\boldsymbol{\sigma}}^{(Q)}$ is defined as the unique (x_1, x_2)-invariant stress field which balances $\boldsymbol{f}^{(Q)}$. This leads to the following auxiliary problem:

$$\begin{cases} \tilde{\boldsymbol{\sigma}}^{(Q)} \cdot \tilde{\boldsymbol{\nabla}} + 12x_3\dfrac{\tilde{\boldsymbol{Q}}}{h^3} = \tilde{\mathbf{o}}, \text{ where } Q_3 = 0 & \text{(23a)} \\ \tilde{\boldsymbol{\sigma}}^{(Q)} \cdot \tilde{\boldsymbol{e}}_3 = \tilde{\mathbf{o}} \quad \text{for} \quad x_3 = \pm h/2 & \text{(23b)} \end{cases}$$

The (x_1, x_2)-invariant solution of this problem is:

$$\sigma_{\alpha 3}^{(Q)} = -\int_{-\frac{h}{2}}^{x_3} 12z\frac{Q_\alpha}{h^3}dz = \frac{6}{h^3}\left(\frac{h^2}{4} - x_3^2\right)Q_\alpha, \quad \sigma_{\alpha\beta}^{(Q)} = 0 \quad \text{and} \quad \sigma_{33}^{(Q)} = 0$$

This is the original shear stress field derived by Reissner.

[1]The constitutive material is symmetric with respect to (x_1, x_2) plane. This assumption could be released but would compromise the simplicity of the presentation.

4.2.3. Extension to laminates under cylindrical bending

When considering laminated plates, the approach described above does not work any more, because it is not possible to bring out shear forces in $(\tilde{\boldsymbol{\sigma}}^{(M)} \cdot \tilde{\boldsymbol{\nabla}})$. Whitney (1972) overcame this difficulty assuming the plate is under cylindrical bending. This is equivalent to assuming: $Q_1 = M_{11,1}$, $Q_2 = M_{12,1}$, $e_{22} = 0$ and $\chi_{22} = 0$.

Whitney's approach for deriving shear correction factors is still implemented in ABAQUS (2007) under additional assumptions. Compared to exact solutions for cylindrical bending (Pagano, 1969, 1970b), this method gives rather good approximation for overall deflection and shear stresses in laminated plates. Eventually, it has also been generalized to functionally graded materials (Nguyen et al., 2007, 2008) and heterogeneous plates (Cecchi and Sab, 2002, 2007), (Lebée and Sab, 2010c,d) and Isaksson et al. (2007). However, how shear stress should be extended for more complex loadings than cylindrical bending (especially involving torsion) is still an issue.

5. The Bending-Gradient plate theory

5.1. Fields generated by a linear variation of the bending moment

5.1.1. Stress field

Since with laminated plates it is not possible to bring out shear forces with Reissner's approach, we suggest considering a more general shear variable, the full bending gradient: $\mathbf{R} = \boldsymbol{M} \otimes \boldsymbol{\nabla}$ where the third-order tensor $\mathtt{R}_{\alpha\beta\gamma}$ respects $M_{\alpha\beta}$ symmetries ($\mathtt{R}_{\alpha\beta\gamma} = \mathtt{R}_{\beta\alpha\gamma}$). This will release the cylindrical bending assumption for laminated plates. In the following, we resume Section 4.2.2 procedure for deriving shear fields in the case of laminated plates.

We have $\tilde{\boldsymbol{\sigma}}^{(M)} \cdot \tilde{\boldsymbol{\nabla}} = 0$ if $\boldsymbol{M}$ is (x_1, x_2)-invariant. When $\boldsymbol{M}$ is function of x_1 and x_2, we have:

$$\tilde{\boldsymbol{\sigma}}^{(M)} \cdot \tilde{\boldsymbol{\nabla}} = s^{(M)}_{ij\beta\alpha}(x_3) M_{\alpha\beta}(x_1, x_2) \nabla_j = s^{(M)}_{ij\beta\alpha} M_{\alpha\beta,\gamma} \delta_{j\gamma} = s^{(M)}_{i\gamma\beta\alpha} \mathtt{R}_{\alpha\beta\gamma}$$

Again $f^{(\mathtt{R})}_i = s^{(M)}_{i\gamma\beta\alpha} \mathtt{R}_{\alpha\beta\gamma}$ is the force per unit volume generated by first order variations of the bending moment $\mathbf{R}$. Using $\tilde{\boldsymbol{\sigma}}^{(M)}$ definition (Equation 20b) and assuming that each layer follows monoclinic symmetry we identify the force per unit volume as:

$$\boldsymbol{f}^{(\mathtt{R})} = \boldsymbol{c}(x_3) : (\boldsymbol{b} + x_3\, \boldsymbol{d}) \therefore \mathbf{R} \text{ and } f^{(\mathtt{R})}_3 = 0 \tag{24}$$

Then, we define $\tilde{\boldsymbol{\sigma}}^{(\mathtt{R})}$ the 3D stress generated by a (x_1, x_2)-invariant bending gradient $\mathbf{R}$ associated to the localization tensor $s^{(\mathtt{R})}_{ij\alpha\beta\gamma}$ such as $\tilde{\boldsymbol{\sigma}}^{(\mathtt{R})} = \tilde{\boldsymbol{s}}^{(\mathtt{R})} \therefore \mathbf{R}$. Like in the case of homogeneous plate, this stress field is derived through the auxiliary problem:

$$\begin{cases} \tilde{\boldsymbol{\sigma}}^{(\mathtt{R})} \cdot \tilde{\boldsymbol{\nabla}} + \tilde{\boldsymbol{f}}^{(\mathtt{R})} = \tilde{\mathbf{o}} & \text{(25a)} \\ \tilde{\boldsymbol{\sigma}}^{(\mathtt{R})} \cdot \tilde{\boldsymbol{e}}_3 = \tilde{\mathbf{o}} \quad \text{for} \quad x_3 = \pm h/2 & \text{(25b)} \end{cases}$$

The (x_1, x_2)-invariant solution of this problem is easily found, leading to the explicit determination of $\tilde{\boldsymbol{s}}^{(\mathtt{R})}$:

$$s^{(\mathtt{R})}_{\alpha 3\eta\zeta\epsilon}(x_3) = -\int_{-\frac{h}{2}}^{x_3} c_{\alpha\eta\gamma\delta}(z) \left(b_{\delta\gamma\epsilon\zeta} + z\, d_{\delta\gamma\epsilon\zeta} \right) dz \ , \quad s^{(\mathtt{R})}_{\alpha\beta\eta\zeta\epsilon} = 0 \quad \text{and} \quad s^{(\mathtt{R})}_{33\eta\zeta\epsilon} = 0 \tag{26}$$

NB: The integral in the determination of $\tilde{\boldsymbol{\sigma}}^{(\mathtt{R})}$ enforces directly the continuity of shear stress distributions and $\tilde{\boldsymbol{s}}^{(\mathtt{R})}(-h/2) = \tilde{\boldsymbol{s}}^{(\mathtt{R})}(h/2) = 0$ ensures the traction free boundary condition on the upper and lower faces of the plate.

5.1.2. Displacement field

Following a procedure similar to the one suggested by Whitney (1972) it is possible to derive a displacement field related to the bending gradient $\mathbf{R}$. Using the 3D constitutive equation 1b, the strain related to $\mathbf{R}$ is written as:

$$\varepsilon^{(\mathrm{R})}_{\alpha 3} = \frac{S_{\alpha\beta}}{2}\sigma^{(\mathrm{R})}_{\beta 3}, \quad \varepsilon^{(\mathrm{R})}_{\alpha\beta} = 0 \quad \text{and} \quad \varepsilon^{(\mathrm{R})}_{33} = 0 \tag{27}$$

where $\boldsymbol{S} = S_{\alpha\beta} = 4\mathcal{S}_{\alpha 3\beta 3}$ is the out-of-plane shear compliance tensor. Then, neglecting the variations of $\mathbf{R}$, it is possible to integrate this strain field and derive the following displacement field related to $\mathbf{R}$:

$$u^{(\mathrm{R})}_{\alpha} = \left(\int_{-\frac{h}{2}}^{x_3} S_{\alpha\zeta}(z) s^{(\mathrm{R})}_{\zeta 3\beta\gamma\delta}(z) dz + \mathcal{k}^{(\mathrm{R})}_{\alpha\beta\gamma\delta} \right) \mathrm{R}_{\delta\gamma\beta}, \quad u^{(\mathrm{R})}_{3} = 0 \tag{28}$$

where $\mathcal{k}^{(\mathrm{R})}_{\alpha\beta\gamma\delta}$ is a fourth order tensor following one minor symmetry: $\mathcal{k}^{(\mathrm{R})}_{\alpha\beta\gamma\delta} = \mathcal{k}^{(\mathrm{R})}_{\alpha\beta\delta\gamma}$. $\boldsymbol{\mathcal{k}}^{(\mathrm{R})}$ is an integration constant which is set by enforcing $\left\langle u^{(\mathrm{R})}_{\alpha} \right\rangle = 0$. Then, we introduce the displacement localization $\boldsymbol{v}^{(\mathrm{R})}$ by:

$$\boldsymbol{u}^{(\mathrm{R})} = \boldsymbol{v}^{(\mathrm{R})} \therefore \mathbf{R}, \quad u^{(\mathrm{R})}_{3} = 0 \tag{29}$$

Finally $\tilde{\boldsymbol{u}}^{(\mathrm{R})}$ is a continuous displacement field.

5.2. Compatible fields for the full bending gradient

In Section 5.1.1, we have derived a localization tensor $\tilde{\boldsymbol{s}}^{(\mathrm{R})}$ which depends on all bending gradient components: $\mathrm{R}_{\alpha\beta\gamma} = M_{\alpha\beta,\gamma}$. Accordingly we define a new approximation of stress fields involving all bending gradient components:

$$\tilde{\boldsymbol{\sigma}}^{BG} = \tilde{\boldsymbol{\sigma}}^{(N)} + \tilde{\boldsymbol{\sigma}}^{(M)} + \tilde{\boldsymbol{\sigma}}^{(\mathrm{R})}$$

and a new stress energy density similar to Definition 15:

$$w^{*BG}(\boldsymbol{N}, \boldsymbol{M}, \mathbf{R})$$

Actually $\tilde{\boldsymbol{\sigma}}^{BG}$ approximation for 3D stress fields is a higher-order gradient theory, as described in Boutin (1996) for 3D continuum and Buannic and Cartraud (2001a) for periodic beams. However, to be consistent with higher-order theories, we should have taken into account the gradient of other static unknowns such as the membrane stress gradient for instance. It is the choice of the authors in the present work to limit the number of static variables only to those which have a contribution to the macroscopic equilibrium of the plate. Thus the number of unknowns remains limited and adapted to engineering applications, contrary to asymptotic expansions and other rigorous approaches in which no distinction is made between significant static unknowns.

Now it is possible to design a complete plate model.

5.2.1. Bending gradient statically compatible fields

Generalized stress. The full bending gradient $\mathbf{R}$ has six components (R_{111}, R_{221}, R_{121}, R_{112}, R_{222}, R_{122}) whereas $\boldsymbol{Q}$ has two components. Since only $(\boldsymbol{N}, \boldsymbol{M}, \boldsymbol{Q})$ appeared in Reissner-Mindlin statically compatible fields, SC^{RM}, while integrating 3D equilibrium equation (1a) through the thickness in Section 4.1, using the full bending gradient as static unknown introduces four static unknowns which *a priori* are not related to plate equilibrium (13).

Let us derive generalized stresses associated to $\tilde{\boldsymbol{\sigma}}^{(\mathrm{R})}$. Using Equation 26 and integrating by parts when necessary leads to:

$$\left\langle \sigma^{(\mathrm{R})}_{\alpha\beta} \right\rangle = 0, \qquad \left\langle x_3 \sigma^{(\mathrm{R})}_{\alpha\beta} \right\rangle = 0, \qquad \left\langle s^{(\mathrm{R})}_{\alpha 3\beta\gamma\delta} \right\rangle = \mathcal{i}_{\alpha\beta\gamma\delta} \tag{30}$$

and we have: $\left\langle \sigma^{(\mathrm{R})}_{\alpha 3} \right\rangle = \boldsymbol{i} \therefore \mathbf{R} = \boldsymbol{Q}$. Only $\boldsymbol{Q}$ remains after integrating $\tilde{\boldsymbol{\sigma}}^{(\mathrm{R})}$ through the thickness and the four other static unknowns are self-equilibrated stress. These stresses are analogous to bimoment and warping functions in the theory of beams under torsion from Vlasov (1961). More precisely we have:

R_{111} and R_{222} are the cylindrical bending part of shear forces Q_1 and Q_2, R_{121} and R_{122} are the torsion part of shear forces and R_{112} and R_{221} are linked to strictly self-equilibrated stresses.

	$\mathtt{R}_{111}$	$\mathtt{R}_{221}$	$\mathtt{R}_{121}$	$\mathtt{R}_{112}$	$\mathtt{R}_{222}$	$\mathtt{R}_{122}$
σ_{13}	$\left\langle s^{(\mathtt{R})}_{13111}\right\rangle = 1$	$\left\langle s^{(\mathtt{R})}_{13122}\right\rangle = 0$	$\left\langle s^{(\mathtt{R})}_{13121}\right\rangle = 0$	$\left\langle s^{(\mathtt{R})}_{13211}\right\rangle = 0$	$\left\langle s^{(\mathtt{R})}_{13222}\right\rangle = 0$	$\left\langle s^{(\mathtt{R})}_{13221}\right\rangle = 1/2$
σ_{23}	$\left\langle s^{(\mathtt{R})}_{23111}\right\rangle = 0$	$\left\langle s^{(\mathtt{R})}_{23122}\right\rangle = 0$	$\left\langle s^{(\mathtt{R})}_{23121}\right\rangle = 1/2$	$\left\langle s^{(\mathtt{R})}_{23211}\right\rangle = 0$	$\left\langle s^{(\mathtt{R})}_{23222}\right\rangle = 1$	$\left\langle s^{(\mathtt{R})}_{23221}\right\rangle = 0$

Bending gradient equilibrium equations. Two observations lead to the definition of statically compatible fields for the bending gradient SC^{BG}. The first one is that we chose $\mathtt{R}$ such as $\boldsymbol{M} \otimes \boldsymbol{\nabla} = \mathtt{R}$ in Section 5.1.1. The second one is that we have $\boldsymbol{Q} = \boldsymbol{i} \therefore \mathtt{R}$. Adapting SC^{RM} fields (13) we suggest the following definition of SC^{BG}:

$$(\boldsymbol{N}, \boldsymbol{M}, \mathtt{R}) \in SC^{BG} \Leftrightarrow \begin{cases} \boldsymbol{N} \cdot \boldsymbol{\nabla} = \mathbf{o} \text{ on } \omega & \text{(31a)} \\ \boldsymbol{M} \otimes \boldsymbol{\nabla} - \mathtt{R} = \mathbf{0} \text{ on } \omega & \text{(31b)} \\ \boldsymbol{i} \therefore \mathtt{R} \cdot \boldsymbol{\nabla} + p_3 = 0 \text{ on } \omega & \text{(31c)} \end{cases}$$

5.2.2. Bending gradient kinematically compatible fields

Dual variables. Taking the derivative of $w^{*BG}(\boldsymbol{N}, \boldsymbol{M}, \mathtt{R})$ with respect to each static unknown leads to the following definition of dual variables:

$$\boldsymbol{e} = \frac{\partial w^{*BG}}{\partial \boldsymbol{N}}, \quad \boldsymbol{\chi} = \frac{\partial w^{*BG}}{\partial \boldsymbol{M}}, \quad \boldsymbol{\Gamma} = \frac{\partial w^{*BG}}{\partial \mathtt{R}} \tag{32}$$

where $\boldsymbol{e}$ is associated to membrane strains and $\boldsymbol{\chi}$ to curvatures. $\boldsymbol{\Gamma}$ is a generalized shear strain. $\boldsymbol{\Gamma}$ is a third-order 2D tensor following $\mathtt{R}$ symmetry: $\Gamma_{\beta\alpha\gamma} = \Gamma_{\alpha\beta\gamma}$.

Internal work for the bending gradient plate model is accordingly written as:

$$V^{BG}_{int} = \int_\omega \boldsymbol{N} : \boldsymbol{e} + \boldsymbol{M} : \boldsymbol{\chi} + {}^t\mathtt{R} \therefore \boldsymbol{\Gamma} d\omega \tag{33}$$

Dualization of bending gradient equilibrium equations. Since SC^{BG} is defined, it is very classical to identify kinematically compatible fields KC^{BG} by integrating by parts the equilibrium equations (31) multiplied with *ad hoc* test fields $\tilde{\boldsymbol{U}}$ and $\boldsymbol{\Phi}$, where $\tilde{\boldsymbol{U}}(x_1, x_2)$ is a 3D vector and $\boldsymbol{\Phi}(x_1, x_2)$ a third-order 2D tensor following $\mathtt{R}$ symmetry: $\Phi_{\beta\alpha\gamma} = \Phi_{\alpha\beta\gamma}$. Detailed computation is given in Appendix A.1. This leads to the weak formulation of the plate theory:

$$V^{BG}_{int} = V^{BG}_{ext}$$

where

$$V^{BG}_{int} = \int_\omega \boldsymbol{N} : (\boldsymbol{i} : (\boldsymbol{U} \otimes \boldsymbol{\nabla})) + \boldsymbol{M} : (\boldsymbol{\Phi} \cdot \boldsymbol{\nabla}) + {}^t\mathtt{R} \therefore (\boldsymbol{\Phi} + \boldsymbol{i} \cdot \boldsymbol{\nabla} U_3)\, d\omega \tag{34}$$

$$V^{BG}_{ext} = \int_\omega p_3 U_3 d\omega + \int_{\partial\omega} (\boldsymbol{N} \cdot \boldsymbol{n}) \cdot \boldsymbol{U} + \boldsymbol{M} : (\boldsymbol{\Phi} \cdot \boldsymbol{n}) + (\boldsymbol{i} \therefore \mathtt{R} \cdot \boldsymbol{n})\, U_3 dl \tag{35}$$

and $\boldsymbol{n}$ is the in-plane unit vector outwardly normal to ω.

Dual strains are identified in V^{BG}_{int} as:

$$\boldsymbol{e} = \boldsymbol{i} : (\boldsymbol{U} \otimes \boldsymbol{\nabla}), \quad \boldsymbol{\chi} = \boldsymbol{\Phi} \cdot \boldsymbol{\nabla}, \quad \boldsymbol{\Gamma} = \boldsymbol{\Phi} + \boldsymbol{i} \cdot \boldsymbol{\nabla} U_3 \tag{36}$$

where $\boldsymbol{\Phi}$ is a generalized rotation and $\boldsymbol{e}$ is exactly the Kirchhoff-Love membrane strain. Since we have assumed the plate is clamped, there is no external work on the edge $\partial\omega$ in V^{BG}_{ext} (Equation 35). This leads to the following condition on $\tilde{\boldsymbol{U}}$ and $\boldsymbol{\Phi}$ for clamped edges:

$$\boldsymbol{\Phi} \cdot \boldsymbol{n} = \mathbf{o} \text{ on } \partial\omega, \qquad \tilde{\boldsymbol{U}} = \tilde{\mathbf{o}} \text{ on } \partial\omega$$

The above remarks enable us to define the set of kinematically compatible fields KC^{BG} for clamped plates:

$$(\boldsymbol{e}, \boldsymbol{\chi}, \boldsymbol{\Gamma}) \in KC^{BG} \Leftrightarrow \begin{cases} \boldsymbol{e} = \boldsymbol{i} : (\boldsymbol{U} \otimes \boldsymbol{\nabla}) \text{ on } \omega & \text{(37a)} \\ \boldsymbol{\chi} = \boldsymbol{\Phi} \cdot \boldsymbol{\nabla} \text{ on } \omega & \text{(37b)} \\ \boldsymbol{\Gamma} = \boldsymbol{\Phi} + \boldsymbol{i} \cdot \boldsymbol{\nabla} U_3 \text{ on } \omega & \text{(37c)} \\ \boldsymbol{\Phi} \cdot \boldsymbol{n} = \mathbf{o} \text{ on } \partial\omega & \text{(37d)} \\ \tilde{\boldsymbol{U}} = \tilde{\mathbf{o}} \text{ on } \partial\omega & \text{(37e)} \end{cases}$$

Localization of displacement. Assuming $\boldsymbol{\Gamma} = 0$ in KC^{BG} leads to $\boldsymbol{\Phi} = -\boldsymbol{i} \cdot \boldsymbol{\nabla} U_3$ and therefore $\chi_{\alpha\beta} = \Phi_{\alpha\beta\gamma} \nabla_\gamma = -U_{3,\alpha\beta} = \kappa_{\alpha\beta}$ coincides with the Kirchhoff-Love definition of curvatures. It is then possible to rewrite the Bending-Gradient curvature as the sum of two terms, $\boldsymbol{\chi} = \boldsymbol{\kappa} + \boldsymbol{\Gamma} \cdot \boldsymbol{\nabla}$, the first order Kirchhoff-Love curvature and the second order contribution of the generalized shear strains $\boldsymbol{\Gamma}$. Based on this observation, we suggest the following definition of in-place displacement localization fields:

$$\boldsymbol{u}^{BG} = \boldsymbol{U} - x_3 \boldsymbol{\nabla} U_3 + \boldsymbol{v}^{(\mathrm{R})} \therefore \mathbb{F} \therefore \boldsymbol{\Gamma} \tag{38}$$

where $\mathbb{F}$ is the generalized shear stiffness introduced in next section. This definition clearly separates first order and second order contributions to in-plane displacement.

5.3. Bending gradient constitutive equations

We have just derived statically and kinematically compatible fields. There remains to derive constitutive equations to get a complete plate theory.

5.3.1. Bending gradient stress energy density

A detailed analysis dedicated to material symmetries is provided in Appendix A.2. The main result is that material symmetry of the plate constituents with respect to (x_1, x_2) plane uncouples Kirchhoff-Love $(\boldsymbol{M}, \boldsymbol{N})$ and shear unknowns $(\mathbf{R})$. Since this is true for almost all laminated plates of interest, we restrict the analysis to this case. This means that the energy density can be written as the sum of two terms:

$$w^{*BG} = w^{*BG,KL}(\boldsymbol{N}, \boldsymbol{M}) + w^{*BG,\mathbf{R}}(\mathbf{R})$$

According to Definition 15, the shear part of the stress energy density is:

$$w^{*BG,\mathbf{R}}(\mathbf{R}) = \frac{1}{2} \int_{-\frac{h}{2}}^{\frac{h}{2}} {}^t\left(\tilde{\boldsymbol{s}}^{(\mathrm{R})} \therefore \mathbf{R}\right) : \tilde{\boldsymbol{\mathcal{S}}}(x_3) : \left(\tilde{\boldsymbol{s}}^{(\mathrm{R})} \therefore \mathbf{R}\right) dx_3 = \frac{1}{2} {}^t\mathbf{R} \therefore \mathbb{f} \therefore \mathbf{R} \tag{39}$$

where:

$$\mathbb{f} = \left\langle {}^t\left(\tilde{\boldsymbol{s}}^{(\mathrm{R})}\right) : \tilde{\boldsymbol{\mathcal{S}}}(x_3) : \tilde{\boldsymbol{s}}^{(\mathrm{R})} \right\rangle \tag{40}$$

Inserting $\tilde{\boldsymbol{s}}^{(\mathrm{R})}$ (Equation 26) into $\mathbb{f}$ definition leads to:

$$\mathbb{f}_{\alpha\beta\gamma\delta\epsilon\zeta} = \int_{-\frac{h}{2}}^{\frac{h}{2}} 4 s^{(\mathrm{R})}_{\phi 3\gamma\beta\alpha}(x_3) \mathcal{S}_{\phi 3\psi 3}(x_3) s^{(\mathrm{R})}_{\psi 3\delta\epsilon\zeta}(x_3) dx_3 \tag{41}$$

which becomes:

$$\mathbb{f} = \int_{-\frac{h}{2}}^{\frac{h}{2}} \left(\int_{-\frac{h}{2}}^{x_3} \left({}^t\boldsymbol{b} + z\, \boldsymbol{d} \right) : \boldsymbol{c}(z) dz \right) \cdot \boldsymbol{S}(x_3) \cdot \left(\int_{-\frac{h}{2}}^{x_3} \boldsymbol{c}(z) : (\boldsymbol{b} + z\, \boldsymbol{d})\, dz \right) dx_3 \tag{42}$$

where $\boldsymbol{S} = S_{\alpha\beta} = 4\mathcal{S}_{\alpha 3\beta 3}$ is the out-of-plane shear compliance tensor.

The generalized shear compliance $\mathbb{f}$ is a sixth-order tensor, with two symmetries. The major symmetry: ${}^t\mathbb{f} = \mathbb{f}$ and the minor symmetries: $\mathbb{f}_{\alpha\beta\gamma\delta\epsilon\zeta} = \mathbb{f}_{\beta\alpha\gamma\delta\epsilon\zeta}$. The identity for these tensors is: $\mathbb{I}_{\alpha\beta\gamma\delta\epsilon\zeta} = i_{\alpha\beta\epsilon\zeta}\,\delta_{\gamma\delta}$. $\mathbb{f}$ definition ensures symmetry and positiveness. However, $\mathbb{f}$ is not always definite since four static degrees of freedom are self-equilibrated stress (like warping is degenerated in the torsion of a beam with a circular section). More details about $\mathbb{f}$ kernel is given in Appendix A.3.

Once the stress energy density is defined, it is straightforward to derive the constitutive equation:

$$\mathbf{\Gamma} = \frac{\partial w^{*BG}}{\partial \mathbf{R}} = \mathbb{f} \therefore \mathbf{R} \tag{43}$$

5.3.2. Bending gradient strain energy density

The strain energy density is defined through the Legendre-Fenchel transform. Thus it necessitates the definition of $\mathbb{f}$ inverse. As indicated previously, $\mathbb{f}$ is not always definite. This is the case for a homogeneous plate. Yet it is possible to be more explicit about $\mathbb{f}$ inverse.

The generalized shear compliance $\mathbb{f}$ maps symmetric third-order tensors on its image:

$$\mathbb{f}: \ \mathbf{R} \in \left(\mathbb{R}^2\right)^3 \longmapsto \mathbb{f} \therefore \mathbf{R} = \mathbf{\Gamma} \in Im\left(\mathbb{f}\right) \subseteq \left(\mathbb{R}^2\right)^3$$

In order to define an inverse for $\mathbb{f}$ we introduce the Moore-Penrose pseudo inverse $\mathbb{F}$ defined as

$$\mathbb{F} = \lim_{\kappa \to 0} \left(\mathbb{f} \therefore \mathbb{f} + \kappa \mathbb{I}\right)^{-1} \therefore \mathbb{f}$$

For instance $\left(\begin{smallmatrix} \lambda & 0 \\ 0 & 0 \end{smallmatrix}\right)$ pseudo inverse is $\left(\begin{smallmatrix} 1/\lambda & 0 \\ 0 & 0 \end{smallmatrix}\right)$. With this definition we have:

$$\mathbb{F}: \ \mathbf{\Gamma} \in \left(\mathbb{R}^2\right)^3 \longmapsto \mathbb{F} \therefore \mathbf{\Gamma} = \mathbf{R} \in Im\left(\mathbb{F}\right) \subseteq \left(\mathbb{R}^2\right)^3$$

Hence $\mathbb{F} \therefore \mathbb{f}$ is the orthogonal projector onto $Im\left(\mathbb{F}\right)$ and $\mathbb{I} - \mathbb{f} \therefore \mathbb{F}$ is the orthogonal projector onto $Ker\left(\mathbb{F}\right)$. Defining an inverse relation for $\mathbb{f}$ imposes to restrain $\mathbb{F}$ domain to $Im\left(\mathbb{f}\right)$: $\left(\mathbb{I} - \mathbb{f} \therefore \mathbb{F}\right) \therefore \mathbf{\Gamma} = \mathbf{0}$. Thus there is an internal constraint over generalized shear strains $\mathbf{\Gamma}$ when $\mathbb{f}$ is not positive definite. Finally, we have the equivalence:

$$\begin{cases} \mathbf{\Gamma} = \mathbb{f} \therefore \mathbf{R} \\ \left(\mathbb{I} - \mathbb{f} \therefore \mathbb{F}\right) \therefore \mathbf{\Gamma} = \mathbf{0} \end{cases} \Leftrightarrow \begin{cases} \mathbf{R} = \mathbb{F} \therefore \mathbf{\Gamma} + \mathbf{R}^k \\ \mathbb{F} \therefore \mathbb{f} \therefore \mathbf{R}^k = \mathbf{0} \end{cases} \tag{44}$$

This enables the definition of the shear part of the strain energy density, using the Legendre-Fenchel transform:

$$w^{BG,\mathbf{\Gamma}}(\mathbf{\Gamma}) = \frac{1}{2}\,{}^t\mathbf{\Gamma} \therefore \mathbb{F} \therefore \mathbf{\Gamma} \quad \text{for } \mathbf{\Gamma} \text{ such that} \quad \left(\mathbb{I} - \mathbb{f} \therefore \mathbb{F}\right) \therefore \mathbf{\Gamma} = \mathbf{0} \tag{45}$$

5.4. Summary of the Bending gradient plate model

Let us summarize all the definitions introduced for the new plate model.

The set of kinematically compatible fields is:

$$(\boldsymbol{e}, \boldsymbol{\chi}, \mathbf{\Gamma}) \in KC^{BG} \Leftrightarrow \begin{cases} \boldsymbol{e} = \boldsymbol{i} : (\boldsymbol{U} \otimes \boldsymbol{\nabla}) \ \text{ on } \omega & \text{(46a)} \\ \boldsymbol{\chi} = \boldsymbol{\Phi} \cdot \boldsymbol{\nabla} \text{ on } \omega & \text{(46b)} \\ \mathbf{\Gamma} = \boldsymbol{\Phi} + \boldsymbol{i} \cdot \boldsymbol{\nabla} U_3 \text{ on } \omega & \text{(46c)} \\ \boldsymbol{\Phi} \cdot \boldsymbol{n} = \mathbf{0} \text{ on } \partial\omega & \text{(46d)} \\ \tilde{\boldsymbol{U}} = \tilde{\mathbf{0}} \text{ on } \partial\omega & \text{(46e)} \end{cases}$$

where $\boldsymbol{e}$ is the conventional in-plane plate strain, $\boldsymbol{\chi}$ is the curvature, $\mathbf{\Gamma}$ is the generalized shear strain and $\boldsymbol{\Phi}$ is the generalized rotation. These fields are almost identical to Reissner-Mindlin kinematically compatible fields but the rotation vector is replaced by the generalized third-order rotation tensor $\boldsymbol{\Phi}$. Assuming $\boldsymbol{\Phi} = \boldsymbol{i} \cdot \boldsymbol{\varphi}$ in 46, where $\boldsymbol{\varphi}$ is a vector representing rotations leads to Reissner-Mindlin-like kinematics: $\boldsymbol{\chi} = \boldsymbol{i} : (\boldsymbol{\varphi} \otimes \boldsymbol{\nabla})$

and $\boldsymbol{\Phi} \cdot \boldsymbol{n} = 0 \Leftrightarrow \boldsymbol{\varphi} = 0$. Thus in the general case, Reissner-Mindlin kinematics can be interpreted as a restriction of $\boldsymbol{\Phi}$ to $\boldsymbol{i} \cdot \boldsymbol{\varphi}$.

The set of statically compatible fields is

$$(\boldsymbol{N}, \boldsymbol{M}, \mathbb{R}) \in SC^{BG} \Leftrightarrow \begin{cases} \boldsymbol{N} \cdot \boldsymbol{\nabla} = \mathbf{o} \text{ on } \omega & (47a) \\ \boldsymbol{M} \otimes \boldsymbol{\nabla} - \mathbb{R} = \mathbf{0} \text{ on } \omega & (47b) \\ (\boldsymbol{i} \therefore \mathbb{R}) \cdot \boldsymbol{\nabla} = -p_3 \text{ on } \omega & (47c) \end{cases}$$

where $\boldsymbol{N}$ is the membrane stress, $\boldsymbol{M}$ is the bending moment and $\mathbb{R}$ the gradient of the bending moment. This set of equations is almost identical to Reissner-Mindlin equations where shear forces have been replaced by the bending gradient $\mathbb{R}$.

Finally, for constitutive material following local monoclinic symmetry with respect to (x_1, x_2) plane (uncoupling between $\mathbb{R}$ and $(\boldsymbol{N}, \boldsymbol{M})$) the Bending-Gradient plate constitutive equations write as:

$$\begin{cases} \boldsymbol{N} = \boldsymbol{\mathcal{A}} : \boldsymbol{e} + \boldsymbol{\mathcal{B}} : \boldsymbol{\chi} & (48a) \\ \boldsymbol{M} = {}^t\boldsymbol{\mathcal{B}} : \boldsymbol{e} + \boldsymbol{\mathcal{D}} : \boldsymbol{\chi} & (48b) \\ \boldsymbol{\Gamma} = \mathbb{f} \therefore \mathbb{R}, \quad \text{where} \quad (\mathbb{I} - \mathbb{f} \therefore \mathbb{F}) \therefore \boldsymbol{\Gamma} = 0 & (48c) \end{cases}$$

The solution of the plate model must comply with the three sets of equations (46, 47, 48).

We recall also variational approaches for the model: solving the static approach of Bending-Gradient consists in finding the set of statically compatible fields $(\boldsymbol{N}, \boldsymbol{M}, \mathbb{R})^{BG}$ which minimizes the complementary potential energy:

$$P^{*BG}\left((\boldsymbol{N}, \boldsymbol{M}, \mathbb{R})^{BG}\right) = \min_{(\boldsymbol{N}, \boldsymbol{M}, \mathbb{R}) \in SC^{BG}} \left\{P^{*BG}\left(\boldsymbol{N}, \boldsymbol{M}, \mathbb{R}\right)\right\} \tag{49}$$

where P^{*BG}, the complementary potential energy of the bending gradient plate problem $\mathcal{P}^{BG}$ is written as:

$$P^{*BG}\left(\boldsymbol{N}, \boldsymbol{M}, \mathbb{R}\right) = \int_\omega w^{*BG}\left(\boldsymbol{N}, \boldsymbol{M}, \mathbb{R}\right) d\omega \tag{50}$$

Again, the strain potential energy of $\mathcal{P}^{BG}$ is:

$$P^{BG}(\boldsymbol{e}, \boldsymbol{\chi}, \boldsymbol{\Gamma}) = \int_\omega w^{BG}(\boldsymbol{e}, \boldsymbol{\chi}, \boldsymbol{\Gamma}) - p_3 U_3 d\omega \tag{51}$$

and solving the kinematic approach of $\mathcal{P}^{BG}$ consists in finding the set of kinematically compatible fields $(\boldsymbol{e}, \boldsymbol{\chi}, \boldsymbol{\Gamma})^{BG}$ which minimizes the strain potential energy under the kinematic constraint $(\mathbb{I} - \mathbb{f} \therefore \mathbb{F}) \therefore \boldsymbol{\Gamma} = \mathbf{0}$:

$$P^{BG}\left((\boldsymbol{e}, \boldsymbol{\chi}, \boldsymbol{\Gamma})^{BG}\right) = \min_{\substack{(\boldsymbol{e}, \boldsymbol{\chi}, \boldsymbol{\Gamma}) \in KC^{BG} \\ (\mathbb{I} - \mathbb{f} \therefore \mathbb{F}) \therefore \boldsymbol{\Gamma} = \mathbf{0}}} \left\{P^{BG}\left(\boldsymbol{e}, \boldsymbol{\chi}, \boldsymbol{\Gamma}\right)\right\} \tag{52}$$

Note that the model presented in this paper for clamped plates can be extended to other boundary conditions as detailed in Appendix A.4.

6. Bending-Gradient or Reissner-Mindlin plate model?

6.1. Homogeneous plate

For a homogeneous plate, the body force becomes

$$\boldsymbol{f}^{(\mathbb{R})} = \frac{12 x_3}{h^3} \boldsymbol{i} \therefore \mathbb{R} \text{ and } f_3^{(\mathbb{R})} = 0 \tag{53}$$

and the bending-gradient localization is

$$s^{(\mathbb{R})}_{\alpha 3 \beta \gamma \delta}(x_3) = \frac{6}{h^3}\left(\frac{h^2}{4} - x_3^2\right) i_{\alpha\beta\gamma\delta}, \quad s^{(\mathbb{R})}_{\alpha\beta\gamma\delta\epsilon} = 0 \quad \text{and } s^{(\mathbb{R})}_{33\gamma\delta\epsilon} = 0 \tag{54}$$

which is exactly the same result as the one from Reissner derived in Section 4.2.2. Moreover, the generalized shear compliance is:

$$\mathbf{f} = \frac{6}{5h}\boldsymbol{i}\cdot\boldsymbol{S}\cdot\boldsymbol{i} \tag{55}$$

and the shear stress energy is:

$$w^{*BG,\mathbf{R}}(\mathbf{R}) = \frac{1}{2}{}^t\mathbf{R}\therefore\boldsymbol{i}\cdot\frac{6}{5h}\boldsymbol{S}\cdot\boldsymbol{i}\therefore\mathbf{R} \tag{56}$$

Since $\boldsymbol{Q} = \boldsymbol{i}\therefore\mathbf{R}$, it is possible to identify there the Reissner-Mindlin stress energy density as:

$$w^{*RM,\boldsymbol{Q}}(\boldsymbol{Q}) = \frac{1}{2}{}^t\boldsymbol{Q}\cdot\frac{6}{5h}\boldsymbol{S}\cdot\boldsymbol{Q}$$

which leads to the Reissner-Mindlin constitutive equation:

$$\boldsymbol{Q} = \frac{5h}{6}\boldsymbol{S}^{-1}\cdot\boldsymbol{\gamma}$$

where $\boldsymbol{\gamma}$ stands here for Reissner-Mindlin plate shear strain. This is the result from Reissner (1945) which exhibits the well-known shear correction factor $k_\alpha = 5/6$. It is furthermore demonstrated in Appendix A.5 that boundary conditions are also identical.

Finally, for homogeneous plates, the Reissner-Mindlin model and the Bending-Gradient model are completely identical.

Moreover, the displacement field suggested in Section 5.2.2 becomes:

$$\boldsymbol{u}^{BG} = \boldsymbol{U} - x_3\boldsymbol{\nabla}U_3 + \frac{5}{4}\left(x_3 - \frac{4x_3^3}{3h^2}\right)\left(\frac{2}{3}\boldsymbol{i}\therefore\boldsymbol{\Phi} + \boldsymbol{\nabla}U_3\right) \tag{57}$$

Identifying $\boldsymbol{\varphi} = \frac{2}{3}\boldsymbol{i}\therefore\boldsymbol{\Phi}$, this is rewritten as:

$$\boldsymbol{u}^{BG} = \boldsymbol{U} + x_3\boldsymbol{\varphi} + \left(\frac{x_3}{4} - \frac{5x_3^3}{3h^2}\right)\boldsymbol{\gamma} \tag{58}$$

with $\boldsymbol{\gamma} = \boldsymbol{\varphi} + \boldsymbol{\nabla}U_3$. This displacement field is very similar to the one chosen by Reddy (1984) in order to build a higher order plate theory. However, in the present case, the second order term in γ involves not only a cubic function of x_3 but also a linear term. This illustrates that refinements in displacement fields does not necessarily follow a Taylor expansion, contrary to many suggestions (Reddy, 1989; Altenbach, 1998).

6.2. Projection of the Bending-Gradient plate model

Since in some cases, the Bending-Gradient is turned into a Reissner-Mindlin plate model, we need a means to estimate the difference between both plate models. For this, we define the projection of the Bending-Gradient model on a Reissner-Mindlin model.

The shear forces energy density in the case of a Reissner-Mindlin plate model writes as:

$$w^{*RM,\boldsymbol{Q}}(\boldsymbol{Q}) = \frac{1}{2}{}^t\boldsymbol{Q}\cdot\boldsymbol{f}^{RM}\cdot\boldsymbol{Q} \tag{59}$$

Since $\boldsymbol{Q} = \boldsymbol{i}\therefore\mathbf{R}$, this stress energy becomes in Bending-Gradient plate model:

$$w^{*BG,\mathbf{R}}(\mathbf{R}) = \frac{1}{2}{}^t\mathbf{R}\therefore\boldsymbol{i}\cdot\boldsymbol{f}^{RM}\cdot\boldsymbol{i}\therefore\mathbf{R} \tag{60}$$

Thus a Reissner-Mindlin compliance $\boldsymbol{f}^{RM}$ is expressed in the Bending-Gradient exactly as for a homogeneous plate (Equation 55):

$$\mathbf{f}^{RM} = \boldsymbol{i}\cdot\boldsymbol{f}^{RM}\cdot\boldsymbol{i} \tag{61}$$

Then, we define the orthogonal projection of a Bending-Gradient compliance tensor $\mathbb{f}$ on a Reissner-Mindlin compliance tensor $\boldsymbol{f}^{RM}$. For this, we introduce the following inner product:

$$\mathbb{f}_{\alpha\beta\gamma\delta\epsilon\zeta}\mathbb{g}_{\alpha\beta\gamma\delta\epsilon\zeta} = {}^t\mathbb{f} \vdots\vdots\vdots \mathbb{g} \tag{62}$$

and the related norm:

$$\|\mathbb{f}\| = \sqrt{{}^t\mathbb{f} \vdots\vdots\vdots \mathbb{f}} \tag{63}$$

We define $\mathbb{f}^{RM}$ the Reissner-Mindlin part of $\mathbb{f}$ as the projection of $\mathbb{f}$ on the linear subspace of tensors writting as $\mathbb{g}^{RM} = \boldsymbol{i} \cdot \boldsymbol{g}^{RM} \cdot \boldsymbol{i}$:

$$\forall \mathbb{g}^{RM}, \quad {}^t\left(\mathbb{f} - \mathbb{f}^{RM}\right) \vdots\vdots\vdots \mathbb{g}^{RM} = 0 \tag{64}$$

which is equivalent to:

$$\forall \boldsymbol{g}^{RM}, \quad {}^t\boldsymbol{f}^{RM} : \boldsymbol{g}^{RM} = {}^t\left(\left(\frac{2}{3}\boldsymbol{i}\right) \therefore \mathbb{f} \therefore \left(\frac{2}{3}\boldsymbol{i}\right)\right) : \boldsymbol{g}^{RM} \tag{65}$$

Thus

$$\boldsymbol{f}^{RM} = \left(\frac{2}{3}\boldsymbol{i}\right) \therefore \mathbb{f} \therefore \left(\frac{2}{3}\boldsymbol{i}\right) \tag{66}$$

defines the projection of $\mathbb{f}$ on Reissner-Mindlin plate model and the Reissner-Mindlin part of $\mathbb{f}$ is:

$$\mathbb{f}^{RM} = \left(\frac{2}{3}\boldsymbol{i} \cdot \boldsymbol{i}\right) \therefore \mathbb{f} \therefore \left(\frac{2}{3}\boldsymbol{i} \cdot \boldsymbol{i}\right) \tag{67}$$

The projection $\boldsymbol{f}^{RM}$ of $\mathbb{f}$ is equivalent to assuming $\mathbb{R} = \frac{2}{3}\boldsymbol{i} \cdot \boldsymbol{Q}$ in $w^{*BG,\mathbb{R}}$ (Equation 39). Actually it is possible to give further mechanical interpretation of this result. Let us consider the following change of generalized shear static variables:

$$Q_\alpha = \mathtt{R}_{\alpha\beta\beta}, \quad \Delta Q_1 = \mathtt{R}_{111} - 2\mathtt{R}_{122}, \quad \Delta Q_2 = 2\mathtt{R}_{121} - \mathtt{R}_{222}, \quad \mathtt{R}_{112} \quad \text{and} \quad \mathtt{R}_{221} \tag{68}$$

In that case the four self-equilibrated static unknowns are ΔQ_1, ΔQ_2, $\mathtt{R}_{112}$, and $\mathtt{R}_{221}$. They are clearly set apart from shear forces Q_α. Setting to zero pure warping unknowns in order to keep only "pure shear forces" leads exactly to $\mathbb{R} = \frac{2}{3}\boldsymbol{i} \cdot \boldsymbol{Q}$. From this, $\mathbb{f}^{RM}$ can be considered as the restriction of $\mathbb{f}$ when setting warping unknowns to zero. Consequently, we introduce the pure warping part of $\mathbb{f}$ as the orthogonal complement of $\mathbb{f}^{RM}$:

$$\mathbb{f}^{\mathrm{W}} = \mathbb{f} - \mathbb{f}^{RM} \tag{69}$$

Finally we suggest the following relative distance between the Bending-Gradient plate model and the Reissner-Mindlin one:

$$\Delta^{RM/BG} = \frac{\|\mathbb{f}^{\mathrm{W}}\|}{\|\mathbb{f}\|} \tag{70}$$

$\Delta^{RM/BG}$ gives an estimate of the pure warping fraction of the shear stress energy and can be used as a criterion for assessing the need of the Bending-Gradient model. When the plate constitutive equation is restricted to a Reissner-Mindlin one, we have exactly $\Delta^{RM/BG} = 0$.

As illustration, we derived $\Delta^{RM/BG}$ for angle-ply laminates which were considered by Pagano (1970a). Each ply is made of unidirectional fiber-reinforced material oriented at θ relative to the direction x_1. All plies have the same thickness and are perfectly bounded. A laminate is denoted between brackets by the successive ply-orientations along the thickness. For instance $[0°, 90°]$ denotes a 2-ply laminate where the lower ply fibers are oriented in the bending direction. The constitutive behavior of a ply is assumed to be transversely isotropic along the direction of the fibers and engineering constants are chosen similar to those of Pagano (1969):

$$E_L = 25 \times 10^6 psi, \quad E_T = E_N = 1 \times 10^6 psi, \quad G_{LT} = G_{LN} = 0.5 \times 10^6 psi,$$

$$G_{NT} = \frac{E_T}{2(1+\nu_{NT})} = 0.4 \times 10^6 psi, \quad \nu_{LT} = \nu_{LN} = \nu_{NT} = 0.25$$

where G_{NT} has been changed to preserve transversely isotropic symmetry. L is the longitudinal direction oriented in the (x_1, x_2) plane at θ with respect to $\tilde{\boldsymbol{e}}_1$, T is the transverse direction and N is the normal direction coinciding with $\tilde{\boldsymbol{e}}_3$

On Figure 2, $\Delta^{RM/BG}$ is plotted for any 2-ply configuration and on Figure 3, for any 4-ply symmetric configurations. It appears clearly that $\Delta^{RM/BG}$, is not negligible (up to 37%). Thus, neglecting warping with a simple Reissner-Mindlin plate model applied to such laminates can lead up to 37% error in the shear stress energy and therefore in the second order deflection.

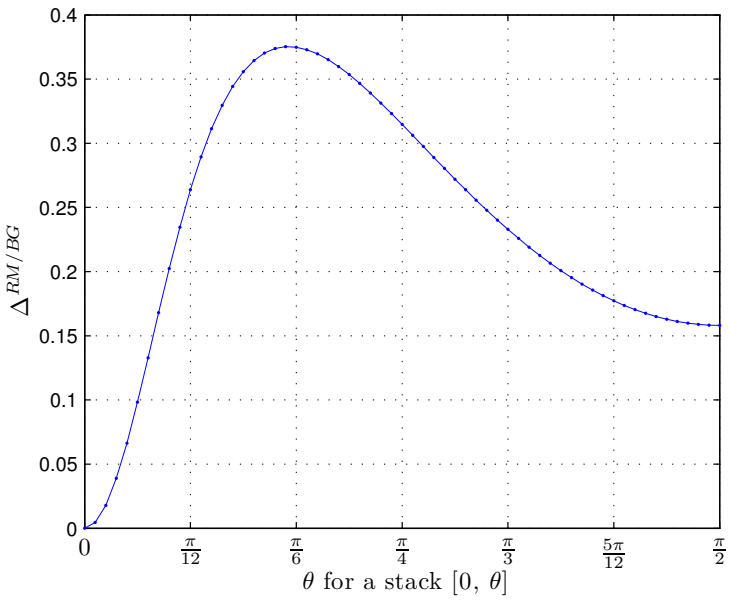

Figure 2: Relative distance between the Reissner-Mindlin and the Bending-Gradient plate models $\Delta^{RM/BG}$ for any 2-ply configuration

7. Conclusion

In this work, applying Reissner's approach for deriving transverse shear stress to a laminated plate revealed that more static shear DOF than the usual shear forces are involved in microscopic fields. Thanks to conventional variational tools, this led to the design of a new higher-order gradient plate theory involving the gradient of the bending moment, instead of shear forces. Statically and kinematically compatible fields as well as constitutive equations were derived. The mechanical meaning of the bending gradient was identified as self-balanced static unknowns associated to warping functions in addition to usual shear forces. The present plate theory does not require any specific constitutive material symmetry and the monoclinic symmetry with respect to plane of $\tilde{\boldsymbol{e}}_3$ normal was introduced only for convenience. We demonstrated also that the Bending-Gradient plate model is the exact extension to laminated plates of the Reissner-Mindlin model originally proposed for homogeneous plates. Finally, we will show in an upcoming paper that the Bending-Gradient model can be used for a higher order homogenization of in-plane periodic plates.

In the second part of this work (Lebée and Sab, 2010a), comparison between models is performed in the cylindrical bending case which makes use of only closed-form solutions. It will be demonstrated that the Bending Gradient model contains most of the relevant aspects of shear effects with very little computation and simple interpretation. The main conclusion is that the Bending-Gradient gives good predictions of both

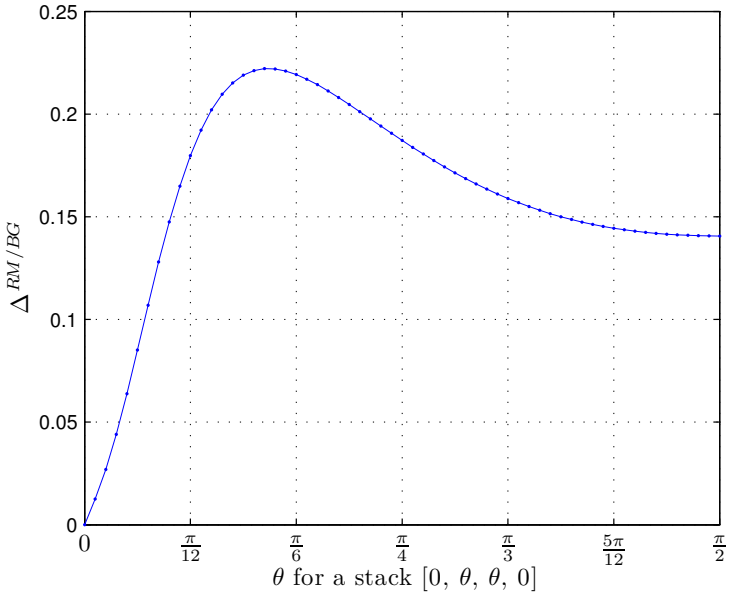

Figure 3: Relative distance between the Reissner-Mindlin and the Bending-Gradient plate models $\Delta^{RM/BG}$ for any symmetric 4-ply configuration

deflection and shear stress distributions in many material configuration and provided the plate follows mirror symmetry ($\boldsymbol{\mathcal{B}} = \boldsymbol{0}$), the Bending-Gradient solution converges to the exact solution when the slenderness ratio h/L goes to 0 faster than other models based on Reissner-Mindlin equations.

A. Appendix

A.1. Dualization

Multiplying 31a with U_α and integrating by parts on the plate domain ω yield:

$$\int_\omega \mathsf{N}_{\alpha\beta} \frac{1}{2} \left(U_{\alpha,\beta} + U_{\beta,\alpha} \right) d\omega = \int_{\partial\omega} \mathsf{N}_{\alpha\beta} n_\beta U_\alpha dl \tag{71}$$

where n_α is the outer normal to $\partial\omega$.

Multiplying 31c with U_3 and integrating by parts on the plate domain ω yield:

$$\int_\omega \mathtt{R}_{\alpha\beta\beta} U_{3,\alpha} d\omega = \int_{\partial\omega} \mathtt{R}_{\alpha\beta\beta} n_\alpha U_3 dl + \int_\omega p_3 U_3 d\omega \tag{72}$$

Multiplying 31b with $\mathtt{\Phi}_{\alpha\beta\gamma}$ and integrating by parts on the plate domain ω yield:

$$\int_\omega \mathsf{M}_{\alpha\beta} \mathtt{\Phi}_{\alpha\beta\gamma,\gamma} + \mathtt{R}_{\alpha\beta\gamma} \mathtt{\Phi}_{\alpha\beta\gamma} d\omega = \int_{\partial\omega} \mathsf{M}_{\alpha\beta} \mathtt{\Phi}_{\alpha\beta\gamma} n_\gamma dl \tag{73}$$

Adding all relations developed above leads to the following expression which is separated into three parts:

$$\begin{aligned} \int_\omega \mathsf{N}_{\alpha\beta} \frac{1}{2} \left(U_{\alpha,\beta} + U_{\beta,\alpha} \right) + \mathsf{M}_{\alpha\beta} \mathtt{\Phi}_{\alpha\beta\gamma,\gamma} + \mathtt{R}_{\alpha\beta\gamma} \left(\mathtt{\Phi}_{\alpha\beta\gamma} + \frac{1}{2} \left(\delta_{\beta\gamma} U_{3,\alpha} + \delta_{\alpha\gamma} U_{3,\beta} \right) \right) d\omega = \\ \int_\omega p_3 U_3 d\omega + \int_{\partial\omega} \mathsf{N}_{\alpha\beta} n_\beta U_\alpha + \mathsf{M}_{\alpha\beta} \mathtt{\Phi}_{\alpha\beta\gamma} n_\gamma + \mathtt{R}_{\alpha\beta\beta} n_\alpha U_3 dl \end{aligned} \tag{74}$$

A.2. Symmetries

First, we derive $\boldsymbol{N}$, $\boldsymbol{M}$ and $\mathbf{R}$ transformation formulas through orthogonal transformations.

Consider a 3D orthogonal transformation $\tilde{\boldsymbol{P}}$ such as $\tilde{\boldsymbol{x}}^{\dagger} = \tilde{\boldsymbol{P}} \cdot \tilde{\boldsymbol{x}}$ is the image of $\tilde{\boldsymbol{x}}$, ($^{t}\tilde{\boldsymbol{P}} \cdot \tilde{\boldsymbol{P}} = \tilde{\boldsymbol{\delta}}$ and $\det \tilde{\boldsymbol{P}} = \pm 1$). A stress field $\tilde{\boldsymbol{\sigma}}$ has the image $\tilde{\boldsymbol{\sigma}}^{\dagger}$ given by:

$$\tilde{\boldsymbol{\sigma}}^{\dagger}(\tilde{\boldsymbol{x}}) = \tilde{\boldsymbol{P}} \cdot \tilde{\boldsymbol{\sigma}}\left({}^{t}\tilde{\boldsymbol{P}} \cdot \tilde{\boldsymbol{x}}\right) \cdot {}^{t}\tilde{\boldsymbol{P}}$$

The analysis is restricted to planar transformations:

$$\tilde{\boldsymbol{P}} = \left(\begin{array}{cc|c} \multicolumn{2}{c|}{\boldsymbol{P}} & \begin{matrix} 0 \\ 0 \end{matrix} \\ \hline 0 & 0 & P_{33}=\pm 1 \end{array}\right)$$

where $\boldsymbol{P}$ is a 2D orthogonal matrix. Then we have:

$$\boldsymbol{N}^{\dagger}(\boldsymbol{x}) = \left\langle \boldsymbol{\sigma}^{\dagger}(\boldsymbol{x}, x_3) \right\rangle = \boldsymbol{P} \cdot \int_{-\frac{h}{2}}^{\frac{h}{2}} \boldsymbol{\sigma}\left({}^{t}\boldsymbol{P} \cdot \boldsymbol{x}, P_{33} x_3\right) dx_3 \cdot {}^{t}\boldsymbol{P} = \boldsymbol{P} \cdot \int_{-P_{33}\frac{h}{2}}^{P_{33}\frac{h}{2}} \boldsymbol{\sigma}\left({}^{t}\boldsymbol{P} \cdot \boldsymbol{x}, y_3\right) \frac{dy_3}{P_{33}} \cdot {}^{t}\boldsymbol{P}$$

This equation does not depend on P_{33} sign. Thus we obtain:

$$\boldsymbol{N}^{\dagger}(\boldsymbol{x}) = \boldsymbol{P} \cdot \int_{-\frac{h}{2}}^{\frac{h}{2}} \boldsymbol{\sigma}\left({}^{t}\boldsymbol{P} \cdot \boldsymbol{x}, x_3\right) dx_3 \cdot {}^{t}\boldsymbol{P} = \boldsymbol{P} \cdot \boldsymbol{N}\left({}^{t}\boldsymbol{P} \cdot \boldsymbol{x}\right) \cdot {}^{t}\boldsymbol{P}$$

The same approach leads to the following equation for the bending moment:

$$\boldsymbol{M}^{\dagger}(\boldsymbol{x}) = P_{33}\boldsymbol{P} \cdot \boldsymbol{M}\left({}^{t}\boldsymbol{P} \cdot \boldsymbol{x}\right) \cdot {}^{t}\boldsymbol{P}$$

We have also, $\mathbf{R} = \boldsymbol{M} \otimes \boldsymbol{\nabla}$. Thus taking the gradient of the previous equation leads to:

$$\mathrm{R}^{\dagger}_{\alpha\beta\gamma}(x_\eta) = P_{33} P_{\alpha\delta} P_{\beta\epsilon} P_{\gamma\zeta} \mathrm{R}_{\delta\epsilon\zeta}\left(P_{\theta\eta} x_\theta\right)$$

When $\tilde{\boldsymbol{P}}$ is diagonal, the above transformation equations simplify. For instance, we have:

$$M^{\dagger}_{\alpha\beta}(\boldsymbol{x}) = \epsilon^{\tilde{P}}_{M_{\alpha\beta}} M_{\alpha\beta}\left({}^{t}\boldsymbol{P} \cdot \boldsymbol{x}\right)$$

where $\epsilon^{\tilde{P}}_{M_{\alpha\beta}} = \pm 1$ is the symmetry index of $M_{\alpha\beta}$ with respect to $\tilde{\boldsymbol{P}}$. For instance $\epsilon^{\tilde{P}}_{N_{\alpha\beta}} = 1$ indicates that $N_{\alpha\beta}$ is symmetric with respect to $\tilde{\boldsymbol{P}}$ and $\epsilon^{\tilde{P}}_{\mathrm{R}_{\alpha\beta\gamma}} = -1$ indicates that $\mathrm{R}_{\alpha\beta\gamma}$ is skew-symmetric with respect to $\tilde{\boldsymbol{P}}$. Finally, it is possible to use all the previous transformation equations to derive the transformation of the stress energy. In the case $\tilde{\boldsymbol{P}}$ reflects a material symmetry, this energy remains invariant. As a consequence, two components having opposite symmetry indexes with respect to $\tilde{\boldsymbol{P}}$ are uncoupled

Table 1 summarizes symmetry indexes for three main symmetries. A major observation is that material invariance through π rotation around $\tilde{\boldsymbol{e}}_3$ axis (case a) ensures uncoupling between shear degrees of freedom $\mathbf{R}$ and Love Kirchhoff degrees of freedom $\boldsymbol{N}$, and $\boldsymbol{M}$. A plate where for all values of x_3 the local behavior is symmetric with respect to (x_1, x_2) plane fulfills the π rotation around $\tilde{\boldsymbol{e}}_3$ symmetry. Thus, uncoupling between $\boldsymbol{N}, \boldsymbol{M}$ and $\mathbf{R}$ holds true also for any kind of laminated plate provided the local constitutive behavior is monoclinic relative to (x_1, x_2) plane (which is the case for fibrous plies).

A.3. Kernel properties of the generalized-shear compliance

In this section we demonstrate that $\mathbb{F} \therefore \mathbf{f} \therefore \boldsymbol{i} = \boldsymbol{i}$ and $\mathbf{f} \therefore \mathbb{F} \therefore \boldsymbol{i} = \boldsymbol{i}$, where $\mathbb{F}$ is Moore-Penrose pseudo inverse. This ensures that the internal constraint $(\mathbb{I} - \mathbf{f} \therefore \mathbb{F}) \therefore \boldsymbol{\Gamma} = \mathbf{0}$ is equivalent to $\boldsymbol{\Phi} = \mathbf{f} \therefore \mathbb{F} \therefore \boldsymbol{\Phi}$.

Proof: Since $\left\langle \boldsymbol{\sigma}^{(\mathrm{R})}_{\alpha 3} \right\rangle = Q_\alpha$, then, $\tilde{\boldsymbol{\sigma}}^{(\mathrm{R})}$ is not uniformly zero through the thickness and $w^{*BG,\mathbf{R}}(\mathbf{R}) > 0$. Thus:

$$\boldsymbol{i} \therefore \mathbf{R} \neq \mathbf{o} \Rightarrow w^{*BG,\mathbf{R}}(\mathbf{R}) > 0 \tag{75}$$

$\tilde{\boldsymbol{P}}$	N_{11}	N_{22}	N_{12}	M_{11}	M_{22}	M_{12}	$\mathtt{R}_{111}$	$\mathtt{R}_{221}$	$\mathtt{R}_{121}$	$\mathtt{R}_{112}$	$\mathtt{R}_{222}$	$\mathtt{R}_{122}$
a) $\begin{pmatrix} -1 & 0 & 0 \\ 0 & -1 & 0 \\ 0 & 0 & 1 \end{pmatrix}$	+	+	+	+	+	+	−	−	−	−	−	−
b) $\begin{pmatrix} 1 & 0 & 0 \\ 0 & 1 & 0 \\ 0 & 0 & -1 \end{pmatrix}$	+	+	+	−	−	−	−	−	−	−	−	−
c) $\begin{pmatrix} 1 & 0 & 0 \\ 0 & -1 & 0 \\ 0 & 0 & 1 \end{pmatrix}$	+	+	−	+	+	−	+	+	−	−	−	+

Table 1: $\epsilon^{\tilde{P}}$ and loads for three main invariances

Let us define: $\mathbf{R}^* = \frac{2}{3}\boldsymbol{i}\cdot\boldsymbol{Q}, \quad \boldsymbol{Q} \neq \mathbf{o}$. We have $\boldsymbol{i} \therefore \mathbf{R}^* = \boldsymbol{Q}$ and then $\mathbf{R}^* \notin Ker\,(\mathbf{f})$. Since $\mathbb{F} \therefore \mathbf{f}$ is the projector on the orthogonal complement of $\mathbf{f}$ kernel, we have:

$$\forall \boldsymbol{Q}, \quad \mathbb{F} \therefore \mathbf{f} \therefore \boldsymbol{i}\cdot\boldsymbol{Q} = \boldsymbol{i}\cdot\boldsymbol{Q}$$

which is the first expected result. The second result is straightforward when noticing that $\mathbf{f}$ and $\mathbb{F}$ have the same kernel: since $\mathbf{f}$ and $\mathbb{F}$ are diagonalizable, we have:

$$\begin{aligned} &\mathbf{R} \in Im\,(\mathbf{f}) \\ \Leftrightarrow\ &\mathbf{R} = \sum_i \mathbf{R}_i \text{ and } \mathbf{f} \therefore \mathbf{R} = \sum_i \lambda_i \mathbf{R}_i, \forall i, \lambda_i \neq 0 \\ \Leftrightarrow\ &\mathbf{R} = \sum_i \mathbf{R}_i \text{ and } \mathbb{F} \therefore \mathbf{R} = \sum_i \mathbf{R}_i/\lambda_i, \forall i, \lambda_i \neq 0 \\ \Leftrightarrow\ &\mathbf{R} \in Im\,(\mathbb{F}) \end{aligned}$$

A.4. Mixed boundary conditions

The edge is separated into two parts: $\partial\omega^k$ where generalized strains $(\tilde{\boldsymbol{U}}^d, \boldsymbol{H}^d)$ are enforced and $\partial\omega^s$ where generalized stress $(\boldsymbol{V}^d, \boldsymbol{M}^d)$ are enforced. $\tilde{\boldsymbol{U}}^d$ is the forced displacement on the edge, $\boldsymbol{H}^d$ is a symmetric second-order tensor related to a forced rotation on the edge, $\boldsymbol{V}^d$ is the force per unit length enforced on the edge and $\boldsymbol{M}^d$ is the full bending moment enforced on the edge

A.4.1. Kinematically compatible fields

We define Bending-Gradient kinematically compatible fields for mixt boundary condition plates as:

$$(\boldsymbol{e}, \boldsymbol{\chi}, \boldsymbol{\Gamma}) \in KC^{BG} \Leftrightarrow \begin{cases} \boldsymbol{e} = \boldsymbol{i} : (\boldsymbol{U} \otimes \boldsymbol{\nabla}) \text{ on } \omega & \text{(76a)} \\ \boldsymbol{\chi} = \boldsymbol{\Phi}\cdot\boldsymbol{\nabla} \text{ on } \omega & \text{(76b)} \\ \boldsymbol{\Gamma} = \boldsymbol{\Phi} + \boldsymbol{i}\cdot\boldsymbol{\nabla} U_3 \text{ on } \omega & \text{(76c)} \\ \boldsymbol{\Phi}\cdot\boldsymbol{n} = \boldsymbol{H}^d \text{ on } \partial\omega^k & \text{(76d)} \\ \tilde{\boldsymbol{U}} = \tilde{\boldsymbol{U}}^d \text{ on } \partial\omega^k & \text{(76e)} \end{cases}$$

The potential energy is:

$$P^{BG}(\boldsymbol{e}, \boldsymbol{\chi}, \boldsymbol{\Gamma}) = \int_\omega w^{BG}(\boldsymbol{e}, \boldsymbol{\chi}, \boldsymbol{\Gamma}) - p_3 U_3 d\omega - \int_{\partial\omega^s} \boldsymbol{V}^d\cdot\boldsymbol{U} + \boldsymbol{M}^d : (\boldsymbol{\Phi}\cdot\boldsymbol{n}) + V_3^d U_3 dl \tag{77}$$

A.4.2. Statically admissible fields

Bending-Gradient statically compatible fields for mixt boundary condition are:

$$(\boldsymbol{N}, \boldsymbol{M}, \mathbf{R}) \in SC^{BG} \Leftrightarrow \begin{cases} \boldsymbol{N} \cdot \boldsymbol{\nabla} = -\boldsymbol{p} \text{ on } \omega & (78a) \\ \boldsymbol{M} \otimes \boldsymbol{\nabla} - \mathbf{R} = 0 \text{ on } \omega & (78b) \\ \boldsymbol{i} \therefore \mathbf{R} \cdot \boldsymbol{\nabla} = -p_3 \text{ on } \omega & (78c) \\ \boldsymbol{N} \cdot \boldsymbol{n} = \boldsymbol{V}^d \text{ on } \partial\omega^s & (78d) \\ \boldsymbol{M} = \boldsymbol{M}^d \text{ on } \partial\omega^s & (78e) \\ \boldsymbol{i} \therefore \mathbf{R} \cdot \boldsymbol{n} = V_3^d \text{ on } \partial\omega^s & (78f) \end{cases}$$

NB: Having $\boldsymbol{M} \cdot \boldsymbol{t} = \boldsymbol{M}^d \cdot \boldsymbol{t}$ on $\partial\omega^s$, where $\boldsymbol{t}$ is orthogonal to $\boldsymbol{n}$ looks unnatural since it involves stresses that do not belong to the edge surface. It is a fourth boundary condition common to higher-order models and related to free edge effects similar to those described in Lebée and Sab (2010b).

The complementary energy is:

$$P^{*BG}(\boldsymbol{N}, \boldsymbol{M}, \mathbf{R}) = \int_\omega w^{*BG}(\boldsymbol{N}, \boldsymbol{M}, \mathbf{R}) d\omega + \int_{\partial\omega^k} (\boldsymbol{N} \cdot \boldsymbol{n}) \cdot \boldsymbol{U}^d + \boldsymbol{M} : \boldsymbol{H}^d + (\mathbf{R} \therefore \boldsymbol{i} \cdot \boldsymbol{n}) U_3^d dl \tag{79}$$

A.5. Degenerated boundary conditions in the homogeneous case

The pseudo inverse in homogeneous case is easy to find:

$$\mathbb{F} = \frac{5h}{6} \frac{4}{9} \boldsymbol{i} \cdot \boldsymbol{S}^{-1} \cdot \boldsymbol{i} \tag{80}$$

and $\mathbf{f} \therefore \mathbb{F} = \frac{2}{3} \boldsymbol{i} \cdot \boldsymbol{i}$. The generalized shear strain, solution of $\mathcal{P}^{BG}$ fulfils $(\mathbb{I} - \mathbf{f} \therefore \mathbb{F}) \therefore \boldsymbol{\Gamma} = 0$, which is equivalent to: $\boldsymbol{\Phi} = \frac{2}{3} \boldsymbol{i} \cdot \boldsymbol{i} \therefore \boldsymbol{\Phi}$ (see Appendix A.3). Then it is possible to rewrite the work of $\boldsymbol{M}$ on the edges $\partial\omega$:

$$\boldsymbol{M} : (\boldsymbol{\Phi} \cdot \boldsymbol{n}) = (\boldsymbol{M} \cdot \boldsymbol{n}) \cdot \left(\frac{2}{3} \boldsymbol{i} \therefore \boldsymbol{\Phi} \right)$$

which is identical to the Reissner-Mindlin work on the edge $\partial\omega$ where the rotation pseudo-vector is $\boldsymbol{\varphi} = \frac{2}{3} \boldsymbol{i} \therefore \boldsymbol{\Phi}$.

References

ABAQUS, 2007. ABAQUS theory manual, version 6.7. ABAQUS.

Altenbach, H., May 1998. Theories for laminated and sandwich plates. a review. Mechanics of Composite Materials 34 (3), 243–252.

Ambartsumian, S., 1969. Theory of anisotropic plates. Ashton Technomic Publishing Co, translated from Russian by T. Cheron.

Boutin, C., Mar. 1996. Microstructural effects in elastic composites. International Journal Of Solids And Structures 33 (7), 1023–1051.

Buannic, N., Cartraud, P., Oct. 2001a. Higher-order effective modeling of periodic heterogeneous beams. i. asymptotic expansion method. International Journal of Solids and Structures 38 (40-41), 7139–7161.
URL http://www.sciencedirect.com/science/article/B6VJS-43TP9JM-7/2/f294534047362a0262c1cafbdbf47fed

Buannic, N., Cartraud, P., Oct. 2001b. Higher-order effective modeling of periodic heterogeneous beams. ii. derivation of the proper boundary conditions for the interior asymptotic solution. International Journal of Solids and Structures 38 (40-41), 7163–7180.
URL http://www.sciencedirect.com/science/article/B6VJS-43TP9JM-8/2/b87b65d71f0e1484d77a9eb6a9e9272d

Caillerie, D., 1984. Thin elastic and periodic plates. Mathematical Methods in the Applied Sciences 6 (2), 159 – 191.

Caron, J. F., Diaz, A. D., Carreira, R. P., Chabot, A., Ehrlacher, A., May 2006. Multi-particle modelling for the prediction of delamination in multi-layered materials. Composites Science And Technology 66 (6), 755–765.

Caron, J.-F., Sab, K., Aug. 2001. Un nouveau modèle de plaque multicouche épaisse. a new model for thick laminates. Comptes Rendus de l'Académie des Sciences - Series IIB - Mechanics 329 (8), 595–600.
URL http://www.sciencedirect.com/science/article/B6W82-43S5PXK-6/2/bd136f393cb5a0153015054387ba6d1d

Carrera, E., 2002. Theories and finite elements for multilayered, anisotropic, composite plates and shells. Archives Of Computational Methods In Engineering 9 (2), 87–140.

Carrera, E., May 2003. Historical review of zig-zag theories for multilayered plates and shells. Appl. Mech. Rev. 56 (3), 287–308.
URL http://link.aip.org/link/?AMR/56/287/1

Cecchi, A., Sab, K., 2002. Out of plane model for heterogeneous periodic materials: the case of masonry. European Journal of Mechanics - A/Solids 21 (5), 715–746.
URL http://www.sciencedirect.com/science/article/B6VKW-46SGV21-1/2/2b89cfb3cc7f99ed497fbf390fd1540b

Cecchi, A., Sab, K., Sep. 2007. A homogenized reissner-mindlin model for orthotropic periodic plates: Application to brickwork panels. International Journal of Solids and Structures 44 (18-19), 6055–6079.
URL http://www.sciencedirect.com/science/article/B6VJS-4N1T1VS-1/2/d919620a660bf31984dd2242f004ad11

Ciarlet, P. G., Destuynder, P., 1979. Justification of the 2-dimensional linear plate model. Journal De Mecanique 18 (2), 315–344.

Dallot, J., Sab, K., 2008. Limit analysis of multi-layered plates. part ii: Shear effects. Journal Of The Mechanics And Physics Of Solids 56 (2), 581–612.

Diaz Diaz, A., Caron, J.-F., Carreira, R. P., Dec. 2001. Model for laminates. Comptes Rendus de l'Académie des Sciences - Series IIB - Mechanics 329 (12), 873–879.
URL http://www.sciencedirect.com/science/article/B6W82-44RNNDJ-6/2/e596e50c0f033131f22c125aa605c234

Diaz Diaz, A., Caron, J. F., Ehrlacher, A., May 2007. Analytical determination of the modes i, ii and iii energy release rates in a delaminated laminate and validation of a delamination criterion. Composite Structures 78 (3), 424–432.

Hadj-Ahmed, R., Foret, G., Ehrlacher, A., Aug. 2001. Stress analysis in adhesive joints with a multiparticle model of multilayered materials (m4). International Journal Of Adhesion And Adhesives 21 (4), 297–307.

Isaksson, P., Krusper, A., Gradin, P., Sep. 2007. Shear correction factors for corrugated core structures. Composite Structures 80 (1), 123–130.
URL http://www.sciencedirect.com/science/article/B6TWP-4K421KK-8/2/abecfb8a8f630a37922924f310323477

Lebée, A., Sab, K., 2010a. A bending gradient model for thick plates, part II: Closed-form solutions for cylindrical bending. submitted.

Lebée, A., Sab, K., Apr. 2010b. A cosserat multiparticle model for periodically layered materials. Mechanics Research Communications 37 (3), 293–297.
URL http://www.sciencedirect.com/science/article/B6V48-4Y95TX1-1/2/6e88981818134d425cae268adda40a97

Lebée, A., Sab, K., 2010c. Reissner-mindlin shear moduli of a sandwich panel with periodic core material. In: Mechanics of Generalized Continua. Vol. 21 of Advances in Mechanics and Mathematics. Springer New York, pp. 169–177.
URL http://dx.doi.org/10.1007/978-1-4419-5695-8_18

Lebée, A., Sab, K., Sep. 2010d. Transverse shear stiffness of a chevron folded core used in sandwich construction. International Journal of Solids and Structures 47 (18-19), 2620–2629.
URL http://www.sciencedirect.com/science/article/B6VJS-506RCW3-1/2/70a945e9ed2d9b63a1eb91826f306304

Lewinski, T., 1991a. Effective models of composite periodic plates .1. asymptotic solution. International Journal Of Solids And Structures 27 (9), 1155–1172.

Lewinski, T., 1991b. Effective models of composite periodic plates .2. simplifications due to symmetries. International Journal Of Solids And Structures 27 (9), 1173–1184.

Lewinski, T., 1991c. Effective models of composite periodic plates .3. 2-dimensional approaches. International Journal Of Solids And Structures 27 (9), 1185–1203.

Mindlin, R., Mar. 1951. Influence of rotatory inertia and shear on flexural motions of isotropic, elastic plates. Journal of Applied Mechanics 18, 31–38.

Naciri, T., Ehrlacher, A., Chabot, A., Mar. 1998. Interlaminar stress analysis with a new multiparticle modelization of multilayered materials (M4). Composites Science and Technology 58 (3-4), 337–343.
URL http://www.sciencedirect.com/science/article/B6TWT-3VCT890-3/2/8c268c8be97bf620d79000db44514ed2

Nguyen, T. K., Sab, K., Bonnet, G., 2007. Shear correction factors for functionally graded plates. Mechanics of Advanced Materials and Structures 14 (8), 567–575.
URL http://www.informaworld.com/10.1080/15376490701672575

Nguyen, T.-K., Sab, K., Bonnet, G., Mar. 2008. First-order shear deformation plate models for functionally graded materials. Composite Structures 83 (1), 25–36.
URL http://www.sciencedirect.com/science/article/B6TWP-4N9DK2S-1/2/eb8bc31778e4482441c248081538b997

Nguyen, V.-T., Caron, J.-F., Sab, K., 2005. A model for thick laminates and sandwich plates. Composites Science and Technology 65 (3-4), 475 – 489.
URL http://www.sciencedirect.com/science/article/B6TWT-4DXC35K-1/2/a05ad2e465b63e1a5af709a0d56ff9ec

Noor, A. K., Malik, M., Feb. 2000. An assessment of five modeling approaches for thermo-mechanical stress analysis of laminated composite panels. Computational Mechanics 25 (1), 43–58.

Pagano, N., 1969. Exact solutions for composite laminates in cylindrical bending. Journal of Composite Materials 3 (3), 398–411.
URL http://jcm.sagepub.com/cgi/content/abstract/3/3/398

Pagano, N., 1970a. Exact solutions for rectangular bidirectional composites and sandwich plates. Journal of Composite Materials 4 (1), 20–34.
URL http://jcm.sagepub.com/cgi/content/abstract/4/1/20

Pagano, N., 1970b. Influence of shear coupling in cylindrical. bending of anisotropic laminates. Journal of Composite Materials 4 (3), 330–343.
URL http://jcm.sagepub.com/cgi/content/abstract/4/3/330

Pagano, N. J., 1978. Stress fields in composite laminates. International Journal Of Solids And Structures 14 (5), 385–400.

Reddy, J. N., 1984. A simple higher-order theory for laminated composite plates. Journal Of Applied Mechanics-Transactions Of The Asme 51 (4), 745–752.

Reddy, J. N., Sep. 1989. On refined computational models of composite laminates. International Journal For Numerical Methods In Engineering 27 (2), 361–382.

Reissner, E., 1945. The effect of transverse shear deformation on the bending of elastic plates. Journal of Applied Mechanics 12, 68–77.

Touratier, M., 1991. An efficient standard plate-theory. International Journal Of Engineering Science 29 (8), 901–916.

Vidal, P., Polit, O., Jun. 2008. A family of sinus finite elements for the analysis of rectangular laminated beams. Composite Structures 84 (1), 56–72.
URL http://www.sciencedirect.com/science/article/B6TWP-4P5R62W-1/2/a6a0602a4dc92d203fa2216ecdebd0e5

Vlasov, V. Z., 1961. Thin-walled elastic beams. National Science Foundation and Department of Commerce.

Whitney, J., 1969. The effect of transverse shear deformation on bending of laminated plate. Journal of Composite Materials 3, 534–547.

Whitney, J., 1972. Stress analysis of thick laminated composite and sandwich plates. Journal of Composite Materials 6 (4), 426–440.

Yu, W., Hodges, D. H., Volovoi, V. V., Oct. 2002a. Asymptotic construction of reissner-like composite plate theory with accurate strain recovery. International Journal of Solids and Structures 39 (20), 5185–5203.
URL http://www.sciencedirect.com/science/article/B6VJS-46TB8KK-2/2/aeb1ff60c0cdb69a9454b7a5cdd08669

Yu, W., Hodges, D. H., Volovoi, V. V., Oct. 2002b. Asymptotic generalization of reissner-mindlin theory: accurate three-dimensional recovery for composite shells. Computer Methods in Applied Mechanics and Engineering 191 (44), 5087–5109.
URL http://www.sciencedirect.com/science/article/B6V29-46V4RGP-6/2/2ffe45f2b95c3216f04307dcc4087900